neally at intervals of 1 hour (total of 8 injections). Mice were euthanized by cervical dislocation at 1 hour after the last cerulein injection. For L-arginine (L-Arg)–induced acute pancreatitis, L-Arg monohydrochloride (Sigma-Aldrich) was dissolved in saline and administered intraperitoneally in 2 dosages of 4 g/kg spaced 1 hour apart and mice were euthanized 72 hours later.

Statistical Analysis

Mann–Whitney *U* test was used for statistical analysis of the histological scores, and an unpaired Student *t* test was used for other analyses. All statistical analyses were performed with JMP software version 7.0 (SAS Institute Inc., Cary, NC), and values of $P < .05$ were considered to indicate statistical significance. All graphs were drawn using GraphPad Prism 5 for Windows (GraphPad Software Inc., San Diego, CA), and all data are presented as mean ± standard error of mean.

Results

Lymphocyte-Deficient Mice Develop Less Severe Cerulein-Induced Pancreatitis

Although accumulating evidence suggests a critical involvement of immune compartments in the pathogenesis of acute pancreatitis,[11–13] the mechanisms of their migration and activation for development of the disease remain unknown. To clarify these mechanisms, we used a murine model of acute pancreatitis induced by cerulein administration.[13,16] A landmark article by Demols et al[13] emphasized the importance of $CD4^+$ T cells by showing that the disease severity in T-cell–lacking *nu/nu* mice injected with cerulein is significantly decreased compared with that in wild-type (WT) mice in this model. We confirmed that cerulein-injected recombinase-activated gene-2 $(RAG2)^{-/-}$ mice, which lack both T and B cells, developed less severe pancreatitis than similarly treated WT mice (Supplementary Figure 1*A–C*). Notably, however, the serum levels of amylase and lipase in cerulein-administered RAG-$2^{-/-}$ mice were significantly higher than those in PBS-treated RAG-$2^{-/-}$ mice (Supplementary Figure 1*C*).

To investigate the roles of immune cells in this model, we used various gene-knockout mice and mice treated with an anti-asialo GM1 monoclonal antibody (Supplementary Figure 2). However, all the mice injected with cerulein developed comparable levels of pancreatitis to paired littermate controls based on the levels of serum amylase (Supplementary Figure 2), suggesting that the presence of lymph nodes and Th17, T-cell receptor $(TCR)\gamma\delta^+$, natural killer (NK), and natural killer T (NKT) cells play no positive pathological roles in this model. Based on these investigations, we hypothesized that this model involves a much more innate immune system, and moved to further assess the role of antigen-presenting cells (APCs), especially macrophages.

$CD11b^{high}Gr\text{-}1^{low}$ and $CD11b^{high}Gr\text{-}1^{high}$ Subpopulations Are Markedly Increased in the Pancreas of Cerulein-Injected Mice

To segmentalize the APC compartments in the pancreas, we stained pancreatic cells obtained from WT mice administered PBS or cerulein with paired monoclonal antibodies against CD11b/CD11c, CD3/NK1.1, CD4/CD8α, or CD3/TCRγδ. Three representative APC compartments were found in the PBS-administered pancreas: $CD11b^{low}CD11c^{high}$ classical dendritic cells (cDCs), $CD11b^{high}CD11c^{low\text{-}high}$ macrophages, and a small population of $CD11b^{high}CD11c^-$ macrophages/granulocytes (Figure 1*Ai*). Surprisingly, however, the ratio and absolute cell number of the $CD11b^{high}CD11c^-$ population were markedly increased in the pancreas of cerulein-injected mice (PBS, $0.34 \pm 0.03 \times 10^5$ vs cerulein, $12.66 \pm 4.86 \times 10^5$; $P = .019$) (Figure 1*Ai* and *Aii*). The other compartments of APCs in the pancreas of cerulein-injected mice were comparable with those in PBS-administered mice (Figure 1*Ai* and *Aii*). Ratios and absolute cell numbers of other immune compartments, such as $CD4^+$ and $CD8^+$ T, NKT, NK, and $TCR\gamma\delta^+$ T cells, were similar in PBS- and cerulein-administered mice (Figure 1*Ai* and *Aii*).

To separate the emerged $CD11b^{high}CD11c^-$ population in the pancreas after cerulein administration, we stained these cells with monoclonal antibodies against the paired CD11b and Gr-1 (Figure 1*Bi, upper panel*).[17] The major subpopulation of $CD11b^{high}$ cells before cerulein administration was the $CD11b^{high}Gr\text{-}1^-$ subpopulation (hereafter designated S1, *purple*). Although the ratio and absolute cell number of the S1 subpopulation in mice administered cerulein were comparable in the 2 groups, the ratios and absolute cell numbers of both the $CD11b^{high}Gr\text{-}1^{low}$ (S2, *green*) and $CD11b^{high}Gr\text{-}1^{high}$ (S3, *blue*) subpopulations were significantly higher than those in PBS-admin-

Figure 1. Cerulein administration induces marked infiltration of $CD11b^{high}Gr\text{-}1^{low/high}$ cells in the pancreas of cerulein-induced pancreatitis. (*Ai*) Expression of CD11b/CD11c, CD3ε/NK1.1, CD4/CD8α, and CD3ε/TCRγδ on cells isolated from the pancreas of cerulein-injected (*Cerulein*) and PBS-injected (*PBS*) mice. The *boxes* indicate: cDCs, $CD11b^{low}CD11c^{high}$; macrophages, $CD11b^{high}CD11c^{low\text{-}high}$; macrophages/granulocytes, $CD11b^{high}CD11c^-$; NK cells, $CD3^-NK1.1^{high}$; NKT cells, $CD3^+NK1.1^{low}$; $CD4^+$ cells, $CD4^+CD8^-$; $CD8^+$ cells, $CD4^-CD8^+$; and $TCR\gamma\delta^+$ cells, $CD3^+TCR\gamma\delta^+$ cells. Data are representative of 3 independent experiments (5 mice/group). (*Aii*) Absolute cell numbers of each compartment in the pancreas of PBS-injected (*white*) and cerulein-injected (*red*) mice. Data are mean ± standard error of mean (SEM) (n = 7/group). *$P < 0.05$. *Mφ*, macrophages; *cDC*, classical DCs; *Gra*, granulocytes. (*Bi*) Expression of CD11b/Gr-1 (*upper*) and Ly6C/Ly6G (*lower*) on cells isolated from the pancreas of cerulein-injected (*right, Cerulein*) and PBS-injected (*left, PBS*) mice. The *boxes* indicate: S1, $CD11b^{high}Gr\text{-}1^-$; S2, $CD11b^{high}Gr\text{-}1^{low}$; and S3, $CD11b^{high}Gr\text{-}1^{high}$. Cells in the S1 (*purple*), S2 (*green*), and S3 (*blue*) subpopulations correspond to the indicated *dots of the same color* according to the FACSDiva analysis. (*Bii*) Absolute cell numbers of the three subpopulations in the pancreas of PBS- or cerulein-administered mice. Data are mean ± SEM (n = 7/group). *$P < .05$. (*C*) Morphologies of Giemsa-stained cells in the S1, S2, and S3 subpopulations. Data are representative of 2 independent experiments. (*D*) Surface expression of various molecules on the 3 subpopulations. Data are representative of 5 independent experiments. (*E*) Mean fluorescent intensities of CD80 and CD86 on the 3 subpopulations. Data are mean ± SEM (n = 4/group). *$P < .05$. MFI, mean fluorescent intensity; n.s., not significant.

istered mice (Figure 1*Bii*). Furthermore, S2 cells highly expressed Ly6C, but not Ly6G, and S3 cells highly expressed Ly6G, but with dominant Ly6C^{low} or minor Ly6C^{high} expression (Figure 1*Bi, lower panel*). Furthermore, morphologic analyses of sorted cells showed that the S1 and S2 subpopulations were macrophage-like, while the S3 subpopulation was a mixture of granulocyte-like cells with segmented nuclei (Ly6C^{low}) and macrophage-like cells with horseshoe-shaped nuclei (Ly6C^{high}) (Figure 1*C*).

Next, we evaluated the phenotypes of the pancreatic S1, S2, and S3 cells by staining with a third monoclonal antibody. None of the 3 subpopulations from PBS- or cerulein-injected mice expressed CD3, NK1.1, DX5, or B220 (Figure 1*D*). Irrespective of whether PBS or cerulein was injected, S1 and S2 cells expressed F4/80, and S3 cells did not, indicating that S3 cells were nonmacrophages composed of segmented granulocytes (Ly6C^{low}) and macrophage-like myeloid-derived suppressor cells (MDSCs) (Ly6C^{high}).[18] In addition, S1, but not S2, cells expressed CD11c. Thus, S1, S2, and S3 cells represented CD11c^{+} macrophages, CD11c^{-} macrophages, and granulocytes/MDSCs, respectively. Before the injection, Ly6C was not expressed on S1 cells, but was expressed on S2 cells at high levels and on S3 cells at moderate levels. After the injection, a substantial proportion of S1 cells showed up-regulated Ly6C expression, and S2 cells maintained high levels of expression. Interestingly, almost all the S3 cells maintained moderate expression levels of Ly6C, while a small but substantial proportion of these cells expressed Ly6C at high levels. In contrast, Ly6G was preferentially expressed on S3 cells (Figure 1*D*). Although all 3 fractions expressed CD80 and CD86 at low levels in PBS-injected mice, these levels were significantly increased in cerulein-injected mice (Figure 1*E*).

CCR2/CCL2-Dependent Migration of Inflammatory Macrophages Is Involved in Cerulein-Induced Pancreatitis

Given the findings that both S2 and S3 cells were markedly increased in the pancreas of cerulein-injected mice, we attempted to determine whether these subpopulations were pathogenic or protective in the process of pancreatitis development using CCL2 (macrophage chemoattractant protein-1)$^{-/-}$ mice, because CCL2 is a representative chemokine for the migration of monocytes/macrophages, but not granulocytes.[19] Although 2 previous reports showed amelioration of the disease by administration of a plasmid vector containing a dominant-negative mutant CCL2 gene in a rat cerulein-injection model[20] and a chemical blocker of CCL2 in a murine model,[21] these studies did not clarify the precise mechanisms of the effects in terms of the immune compartments. As expected, microscopic analyses revealed that the pathology in terms of the histological score was markedly milder in cerulein-administered CCL2$^{-/-}$ mice than in cerulein-administered WT mice (Figure 2*A* and *B*). Consistent with these findings, the serum amylase and lipase levels were significantly lower in cerulein-administered CCL2$^{-/-}$ mice than in cerulein-administered WT mice (Figure 2*C*). Notably, the ratio and absolute cell number of the S2 subpopulation, but not the S1 and S3 subpopulations, were significantly lower in cerulein-administered CCL2$^{-/-}$ mice than in cerulein-injected WT mice (Figure 2*D* and *E*), suggesting a pathological role of CD11b^{high} Gr-1^{low} S2 macrophages in this model. Interestingly, the expression levels of CD80 and CD86 on S1, S2, and S3 cells after cerulein injection were comparable in the 2 groups (Figure 2*F*), suggesting an independent mechanism for the activation of migrating cells in the pancreas.

Pathological Role of CD11b^{high}Gr-1^{low} Macrophages in Cerulein-Induced Pancreatitis

Next, we used mice depleted of monocytes/macrophages using clodronate before the cerulein challenge to assess the role of macrophages in this model. As expected, clodronate-administered mice developed less severe pancreatitis after cerulein injection compared with control mice based on the histology (Supplementary Figure 3*A*) and the serum levels of amylase and lipase (Supplementary Figure 3*B*), thereby confirming a pathological role of monocytes/macrophages in this cerulein-induced pancreatitis model. Interestingly, the clodronate protocol equally depleted approximately 80% of the S1, S2, and S3 subpopulations (Supplementary Figure 3*C* and *D*). Given the possibility that infiltrating macrophages are critically involved in the pathogenesis of this cerulein-induced pancreatitis model, we investigated whether infiltrating S2 or S3 cells induced pancreatic acinar cell apoptosis in vitro. We found that in vitro cultures with cerulein showed significantly increased ratios of apoptotic acinar cells compared with in vitro cultures without cerulein, and also found that addition of S2, but not S3, cells further increased the ratios of apoptotic cells, irrespective of the numbers of total (Annexin V [AV]$^{+}$ 7-amino actinomycin D$^{+/-}$), early (AV^{+}7-amino actinomycin D-), or late (AV^{+}7-amino actinomycin D^{+}) apoptotic cells. Notably, all S2 cell-induced apoptosis was abolished by the addition of neutralizing anti-tumor necrosis factor-α (TNF-α) monoclonal antibodies (Supplementary Figure 4).

Hemodynamics of Macrophages and Granulocytes in the Pathogenesis of Cerulein-Induced Pancreatitis

To further determine the hemodynamics of the increased numbers of S2 macrophages and S3 granulocytes/MDSCs in this model, we conducted parabiosis surgery between Ly5.1- and Ly5.2-background WT mice. At 2 weeks after the parabiosis surgery, we administered cerulein or PBS by intraperitoneal injection to the parabionts (Figure 3*A*). Before the injection, we confirmed that the proportions of S1 and S2 macrophages in the pancreas were significantly lower than those in the spleen, whereas those of S3 cells were comparable in the pancreas and spleen (Supplementary Figure 5). As expected, neither mouse in group 1 showed any inflammatory changes in

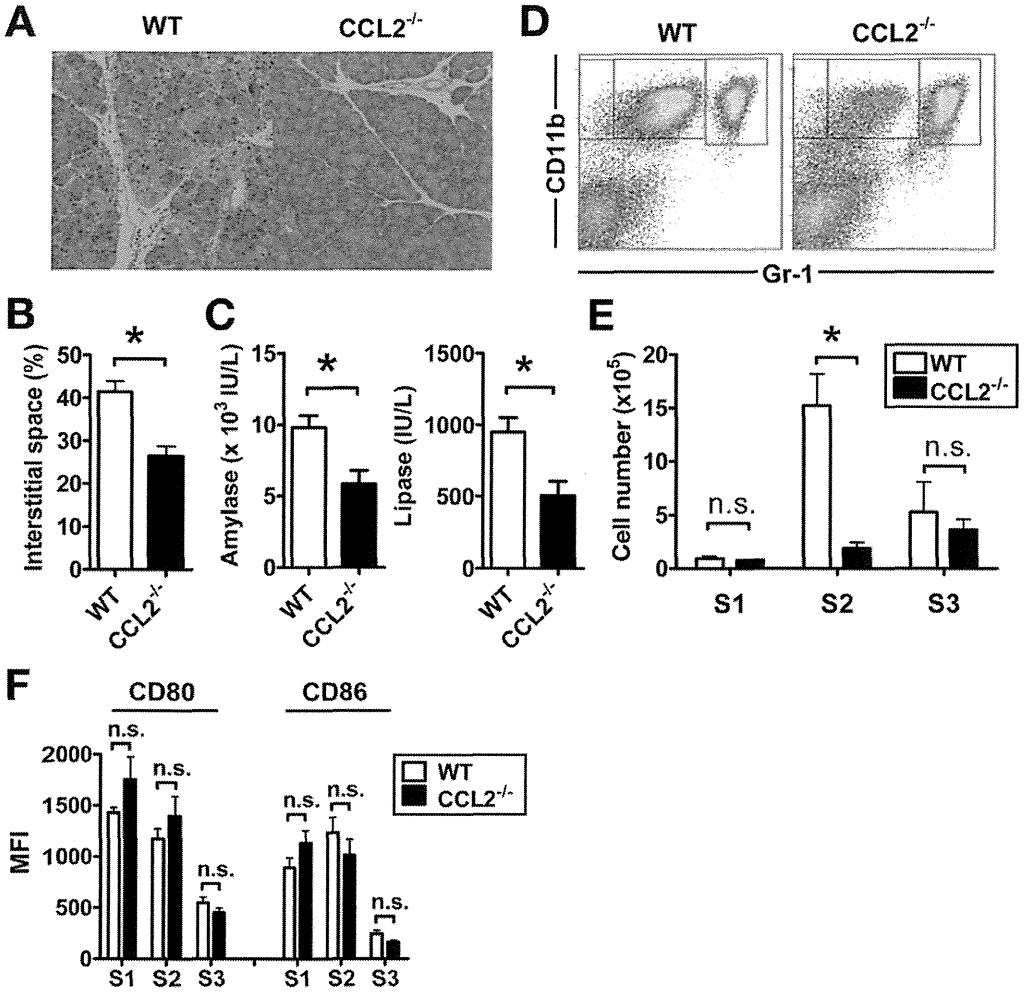

Figure 2. Pancreatitis is ameliorated in cerulein-administered CCL2$^{-/-}$ mice. (*A*) H&E staining of the pancreas in cerulein-administered WT and CCL2$^{-/-}$ mice. Original magnification, ×200. (*B*) Histological scores (n = 5). *$P < .05$. (*C*) Serum amylase and lipase levels (n = 10). *$P < .05$. (*D*) Expression of CD11b/Gr-1 on pancreatic cells of the indicated mice administered cerulein. (*E*) Absolute cell numbers of each subpopulation (n = 4) of the indicated mice administered cerulein. *$P < .05$. (*F*) Mean fluorescence intensities of CD80 and CD86 on each subpopulation (n = 4) of the indicated mice administered cerulein. Data are representative of 2 independent experiments. MFI, mean fluorescent intensity; n.s., not significant.

the pancreas, while both mice in group 2 showed equally inflammatory pathology in the pancreas (Figure 3*B*). Surprisingly, however, only the injected mice of group 3 parabionts showed pathological findings (Figure 3*B*). Consistently, the concentrations of serum amylase and lipase in group 2 and group 3 were significantly higher than those in group 1, and those in group 2 were almost double those in group 3, although the difference was not significant (Figure 3*C*). Furthermore, the absolute cell numbers of the S2 and S3 subpopulations in the pancreas of the cerulein-administered parabionts, but not the PBS-administered parabionts, in group 2 and group 3 were significantly higher than those in group 1 (Figure 3*D* and *E*). However, no significant differences in the absolute cell numbers of the S1 subpopulation were found between any of the 3 groups (Figure 3*D* and *E*). These surprising results indicated that the disease occurs in the injected parabionts only, despite the active circulation of immune cells, suggesting that the mechanism of pancreas damage involves direct translation of cerulein from the peritoneal cavity to the pancreas. To further assess the hemodynamics of the S1, S2, and S3 subpopulations after cerulein injection, we separately assessed host- and donor-derived cells by staining the Ly5.1 and Ly5.2 markers. Consistent with these findings, the homing of donor-derived cells of the S1 and S2 subpopulations was highly restricted at approximately 1:9 to 2:8 compared with that of S3 cells (approximately 1:3) (Figure 3*F*), although the numbers of S2 and S3 cells were increased by almost 70-fold after cerulein injection (Figure 3*E*).

To further assess the role of the CCR2/CCL2 axis in the pathogenesis of this model, we again performed parabiosis surgery between Ly5.1$^+$ WT and Ly5.2$^+$ CCL2$^{-/-}$ mice, and injected both mice with cerulein at 2 weeks after the surgery (Supplementary Figure 6*A*). Consistent with the previous data, CCL2$^{-/-}$ mice developed less severe pancreatitis than WT mice (Supplementary Figure 6*B*) in accordance with the lower infiltration of S2 cells into CCL2$^{-/-}$ mice, but comparable infiltration of S3 cells (Supplementary Figure 6*C* and *D*). Furthermore, irrespective of the diseased WT mice or nondiseased CCL2$^{-/-}$ mice, the percentages of chimerism were <20% in the S1 and S2 subpopulations and <30% in the S3 subpopulation (Supplementary Figure 6*C* and *D*), suggesting that the infiltrating cells were derived from some reservoirs on the host side.

Given the finding that the pancreatitis only occurred in the cerulein-injected parabionts in the parabiosis system, we hypothesized that cerulein damages the pancreas, leading to up-regulation of chemokine expression, and then

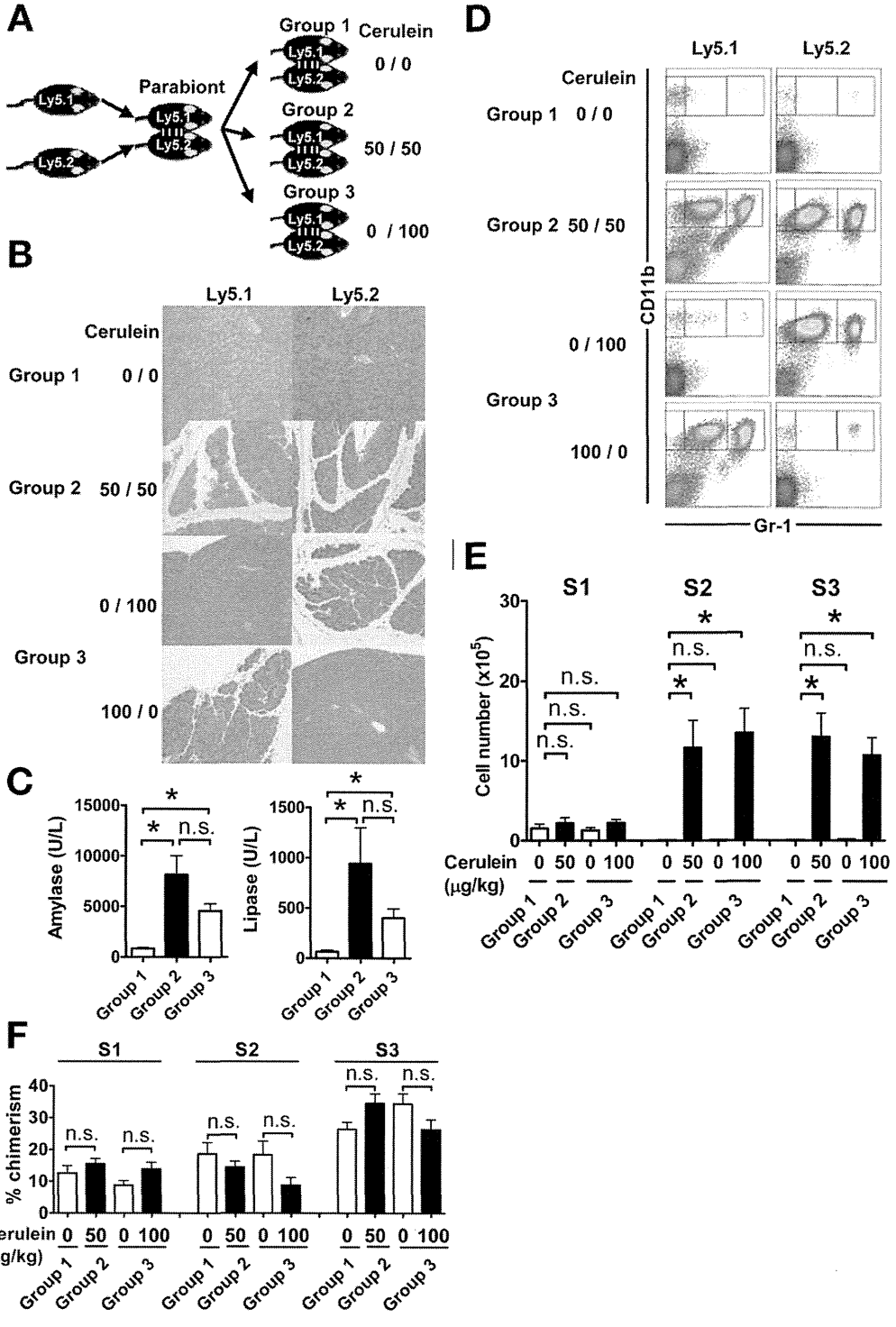

Figure 3. Hemodynamics of pancreatic mononuclear cells. (*A*) Study design. Parabionts were divided into 3 groups. Group 1 (6 pairs), not administered cerulein; group 2 (6 pairs), 50 μg/kg cerulein bilaterally; group 3 (6 pairs), 100 μg/kg cerulein to only 1 partner. (*B*) H&E staining of the pancreas. Original magnification, 200×. (*C*) Serum amylase and lipase levels. *$P < .05$. (*D*) Flow cytometry of CD11b/Gr-1. Data are representative of at least 5 independent experiments. (*E*) Absolute cell numbers of each subpopulation. *$P < .05$. (*F*) Percentages of chimerism of each subpopulation in each group. n.s., not significant.

macrophages/granulocytes/MDSCs in reservoirs migrate to the diseased pancreas. Therefore, we focused on the bone marrow (BM) as a reservoir for migratory macrophages in this model.[22] As expected, the absolute cell number of the CD11b^{high}Gr-1^{low} S2 subpopulation, but not the other subpopulations, in the BM of cerulein-administered mice was significantly lower than that in PBS-administered mice (Supplementary Figure 7). These findings indicate that S2 cells in the BM are mobilized into the injured pancreas after cerulein injection.

Suppressor of Cytokine Signaling 3–Mediated Activation of Macrophages Is Involved in Development of Cerulein-Induced Pancreatitis

Although these results clearly demonstrated that CCR2/CCL2-mediated migration of S2 macrophages to the pancreas is critically involved in the pathogenesis of cerulein-induced pancreatitis, surprisingly, the expression levels of CD80 and CD86 on S1, S2, and S3 cells in the pancreas of cerulein-injected CCL2$^{-/-}$ mice were up-regulated and comparable with those in the pancreas of

cerulein-injected WT mice (Figure 2*F*). This was also the case for cerulein-administered RAG-2$^{-/-}$ mice, which showed marked infiltration of S2 and S3 cells and up-regulation of CD80 and CD86 costimulatory molecules (Supplementary Figure 1*D–F*). These observations suggest that the macrophage activation step (step 2) in the cerulein-injected pancreas is involved in this model, in addition to the macrophage migration step (step 1). Regarding this issue, it was interesting that only interleukin (IL)-6, unlike other proinflammatory cytokines, is protective in this model.[23] It is well known that signal transducer and activation of transcription (STAT)3 activation by IL-6 inhibits nuclear factor−κB (NF-κB) activation, and conversely suppressor of cytokine signaling (SOCS) 3 suppresses STAT3 activation via IL-6.[24] Therefore, we hypothesized that SOCS3 is critically involved in step 2, the activation of pancreatic macrophages, in this model.

We confirmed that SOCS3 was specifically deleted in CD11b$^+$, but not CD11b$^-$, cells isolated from the pancreas of macrophage-specific SOCS3-conditional knockout (SOCS3cKO) mice (Supplementary Figure 8*A*). Consistent with our hypothesis, TNF-α production from splenic lipopolysaccharide (LPS)-stimulated SOCS3cKO CD11b$^+$ cells was significantly lower than that from splenic LPS-stimulated WT CD11b$^+$ cells, while IL-10 production from splenic LPS-stimulated SOCS3cKO CD11b$^+$ cells was significantly higher than that from splenic LPS-stimulated WT CD11b$^+$ cells (Supplementary Figure 8*B*). Interestingly, however, IL-6 production was not affected by the deletion of SOCS3 in CD11b$^+$ cells (Supplementary Figure 8*B*). Furthermore, importantly, the messenger RNA of SOCS3 in pancreatic CD11b$^+$Gr-1^{low} S2 cells from cerulein-injected mice was significantly higher than that from PBS-injected mice, and the messenger RNA of SOCS1 was not affected by the cerulein injection (Supplementary Figure 8*C*).

To further test this hypothesis, we compared age-matched WT and SOCS3cKO mice in this cerulein model. Histological analyses revealed that cerulein-administered SOCS3cKO mice developed significantly milder pancreatitis than control WT mice, based on the histological scores (Figure 4*Ai* and *Aii*). Consistently, the serum concentrations of amylase and lipase in cerulein-administered SOCS3cKO mice were significantly lower than those in control WT mice (Figure 4*B*). The ratios and absolute cell numbers of the S1, S2, and S3 subpopulations were comparable in the 2 groups (Figure 4*C*). In contrast, the up-regulation of CD80 and CD86 on S1 and S2 macrophages, but not on S3 granulocytes/MDSCs, in the pancreas was significantly impaired in cerulein-administered SOCS3cKO mice compared with cerulein-injected WT mice (Figure 4*D*).

Notably, the expression of TNF-α, but not IL-10, in the S1 and S2 subpopulations of pancreatic mononuclear cells from cerulein-injected SOCS3cKO mice after culture in the presence or absence of LPS was markedly impaired compared with paired cells from cerulein-injected WT mice (Figure 4*Ei* and *Eii*). In contrast, the S3 granulocyte/MDSC subpopulations from both WT and SOCS3cKO mice expressed IL-10, but not TNF-α, regardless of culture in the presence or absence of LPS (Figure 4*Ei* and *Eii*), suggesting that this population includes IL-10-expressing MDSCs in addition to granulocytes. Consistent with these results, the phosphorylation of STAT3, but not p38 mitogen-activated protein kinase, in S2 macrophages in the pancreas of cerulein-administered mice was significantly higher than that in the pancreas of PBS-administered mice (Figure 4*Fi* and *Fii*). In a similar experiment using macrophage-specific SOCS1-cKO mice, cerulein-administered WT mice and SOCS1cKO mice similarly developed pancreatitis and showed no detectable significant differences (Supplementary Figure 9*A–F*).

CCR2/CCL2-Mediated Migration of Macrophages Is Involved in Development of L-Arg–Induced Acute Pancreatitis

We further assessed whether the 2-step model (migration and activation of macrophages) is generally accepted in other murine models of acute pancreatitis. To this end, we used an L-Arg–induced acute pancreatitis model.[25] We confirmed the presence of acute pancreatitis accompanied by marked acinar cell damage and infiltration of mononuclear cells (Supplementary Figure 10*A*) and higher serum levels of amylase and lipase (Supplementary Figure 10*B*) in L-Arg–injected mice. Similar to the cerulein model, the ratio and absolute number of the CD11b$^+$Gr-1^{low} S2 subpopulation were markedly increased in the L-Arg model, whereas, unlike the cerulein model, the ratio and absolute number of the CD11b$^+$Gr-1- S1 subpopulation were also significantly increased in the L-Arg model, while the ratio and absolute number of the CD11b$^+$Gr-1^{high} S3 subpopulation were comparable (Figure 5*Ai* and *Aii*). Consistent with the cerulein model, the expression levels of CD80 and CD86 on S1, S2, and S3 cells in the pancreas of L-Arg–injected mice were significantly up-regulated compared with those in the pancreas of PBS-injected WT mice (Figure 5*B*).

Next, we compared WT and CCL2$^{-/-}$ mice in the L-Arg model. As expected, CCL2$^{-/-}$ mice were resistant to the model compared with WT mice based on the histology (Figure 5*Ci*) and serum levels of amylase and lipase (Figure 5*Cii*). The absolute numbers of S1 and S2, but not S3, cells in the pancreas of L-Arg–injected CCL2$^{-/-}$ mice were significantly lower compared with WT mice (Figure 5*Di* and 5*Dii*), while the expression levels of CD80 and CD86 on S1, S2, and S3 cells after L-Arg injection were comparable in the 2 groups (Figure 5*E*). Furthermore, we compared WT and SOCS3cKO mice using the L-Arg model. L-Arg–injected SOCS3cKO mice tended to develop mild pancreatitis compared with L-Arg–injected WT mice in terms of the histology and serum concentrations of amylase and lipase, although the differences were not significant (Supplementary Figure 11*A* and *B*).

Discussion

In this study, we have demonstrated sequential steps of macrophage migration and activation in the pathogenesis of cerulein-induced acute pancreatitis: step 1, CCL2/CCR2-

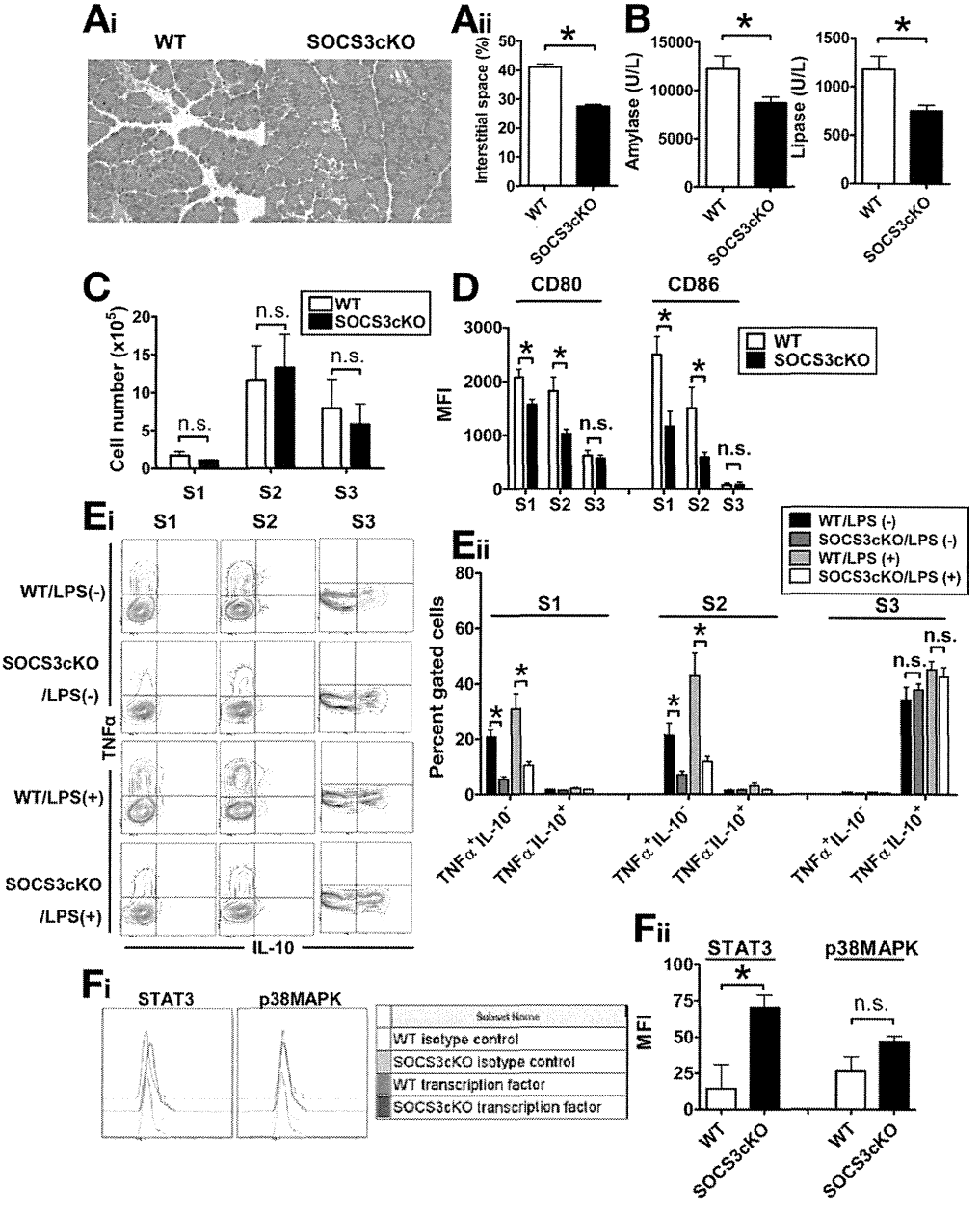

Figure 4. SOCS3 in pancreatic macrophages promotes activation of pancreatic macrophages and enhances the severity of pancreatitis. (*Ai*) H&E staining of the pancreas in cerulein-administered WT and SOCS3cKO mice. Original magnification, ×200. (*Aii*) Histological scores (n = 9). *$P < .05$. (*B*) Serum amylase and lipase levels (n = 9). *$P < .05$. (*C*) Absolute cell numbers of the $CD11b^+Gr\text{-}1^-$ S1, $CD11b^+Gr\text{-}1^{low}$ S2, and $CD11b^+Gr\text{-}1^{high}$ S3 pancreatic subpopulations (n = 3). (*D*) Mean fluorescence intensities of CD80 and CD86 on pancreatic cells (n = 3). *$P < .05$. (*Ei*) Intracellular TNF-α and IL-10 expression with or without LPS stimulation in each subpopulation (n = 4). Data are representative of 2 independent experiments. (*Eii*) Percentages of the indicated cells in each subpopulation. *$P < .05$. (*Fi*) Flow cytometry of STAT3 and p38 mitogen-activated protein kinase phosphorylation in pancreatic S2 macrophages (n = 4). (*Fii*) Percentages of phosphorylation in the S2 subpopulation (n = 4). *$P < .05$. MAPK, mitogen-activated protein kinase; MFI, mean fluorescent intensity; n.s., not significant.

dependent migration of $CD11b^{high}Gr\text{-}1^{low}$ macrophages to the damaged pancreas; and step 2, SOCS3-dependent activation of these macrophages. Thereafter, the activated macrophages might cross talk with still-unidentified acquired immune cells, instructing them to become the eventual effector cells that establish acute pancreatitis.[13] Our immunological scenario for the development of cerulein-induced acute pancreatitis is depicted in Figure 6.

First, we comprehensively analyzed the compartments of immune cells in the pancreas by comparing them under steady-state conditions and during inflammation induced by cerulein administration. Contrary to our expectations, we found that almost all sets of immune compartments for innate and acquired immunity, such as APCs (cDCs and macrophages) and T, NKT, and NK cells, except for the $CD11b^{high}CD11c^-$ population, resided in the normal pancreas. These findings suggest that the immune system might be normally engaged in the maintenance of the pancreas, unlike previous physiological and biochemical visions for the maintenance of pancreatic homeostasis.

Consistent with this view, Demols et al[13] demonstrated that T-cell–deficient *nu/nu* mice do not develop cerulein-induced pancreatitis, and concluded that this model is T-cell–dependent. In this regard, we confirmed that RAG-$2^{-/-}$ mice were resistant to the cerulein model (Supplementary Figure 1). Although these results suggest that T cells are the eventual effectors that establish the pathogenesis of cerulein-induced acute pancreatitis, such hyperacute establishment of this disease seems to be more largely caused by the involvement of innate immune cells, which promptly produce effector cytokines, rather than the involvement of antigen-specific conventional $TCR\gamma\delta^+$ T cells. Based on this hypothesis, we assessed the role of

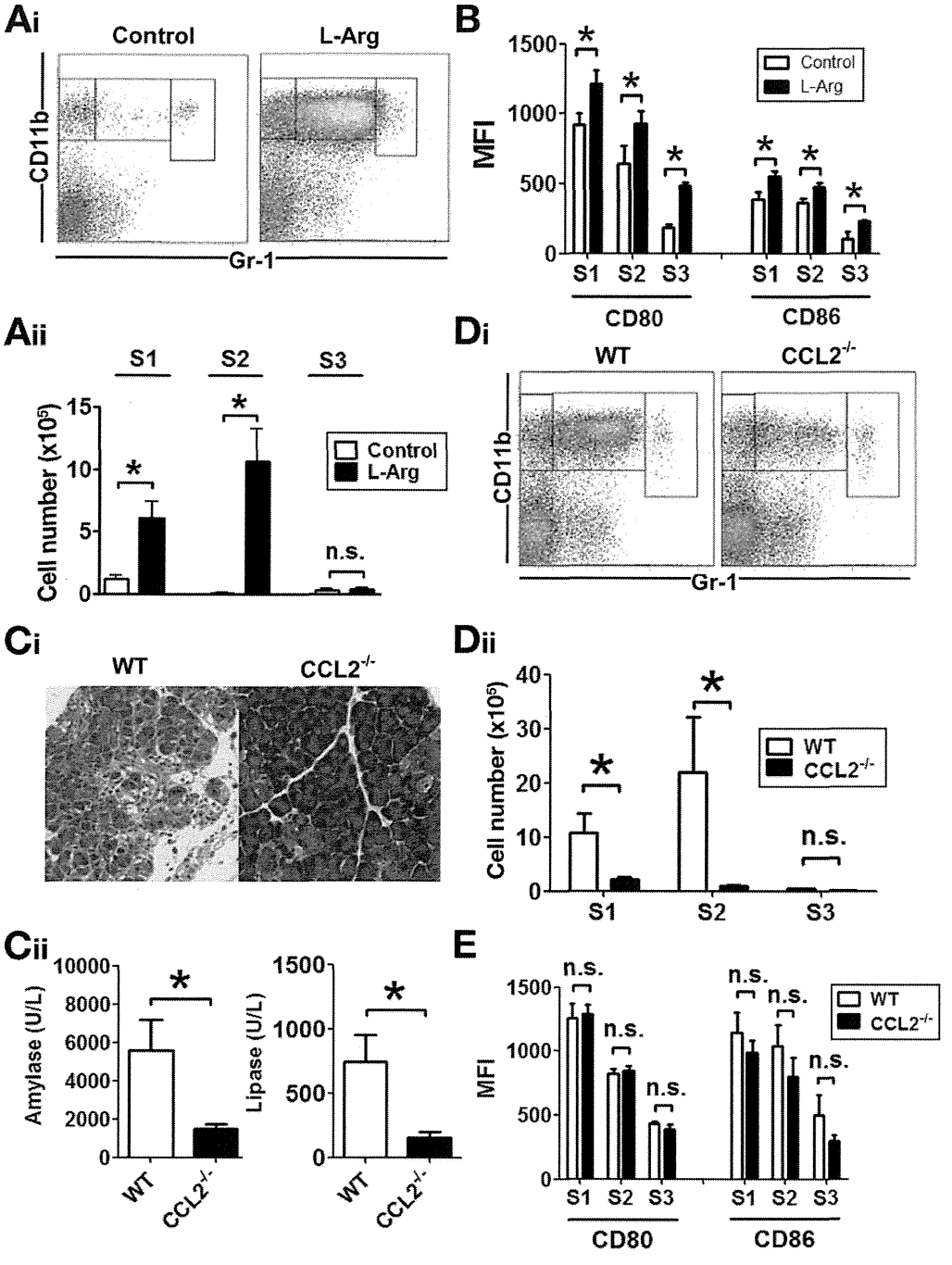

Figure 5. L-Arg–induced acute pancreatitis is mediated by CCL2/CCR2-mediated migration of macrophages. (*Ai*) Expression of CD11b/Gr-1 of cells isolated from the pancreas of L-Arg–injected (*right*) and saline-injected (*left*) mice. The *boxes* indicate: S1, CD11b^{high}Gr-1^{-}; S2, CD11b^{high}Gr-1^{low}; and S3, CD11b^{high}Gr-1^{high}. (*Aii*) Absolute cell numbers of the 3 subpopulations in the pancreas of saline- or L-Arg–administered mice. Data are mean ± standard error of mean (SEM) (n = 4/group). *$P < .05$. (*B*) Mean fluorescence intensities of CD80 and CD86 on the 3 subpopulations. Data are representative of at least 4 independent experiments. Data are mean ± SEM (n = 4/group). *$P < .05$. (*Ci*) H&E staining of the pancreas in L-Arg–administered WT and CCL2$^{-/-}$ mice. Original magnification, ×200. (*Cii*) Serum amylase and lipase levels (n = 5). *$P < .05$. (*Di*) Expression of CD11b/Gr-1 on pancreatic cells of the indicated mice administered L-Arg. (*Dii*) Absolute cell numbers of each subpopulation (n = 5) of the indicated mice administered L-Arg. *$P < .05$. (*E*) Mean fluorescence intensities of CD80 and CD86 on each subpopulation (n = 5) of the indicated mice administered L-Arg. MFI, mean fluorescent intensity; n.s., not significant.

TCR$\gamma\delta^+$ T and NKT cells, which are deleted in RAG-2$^{-/-}$ mice, but are closer to the innate cells than TCR$\gamma\delta^+$ T cells. Unexpectedly, however, TCR$\gamma\delta^{-/-}$ mice and CD1d$^{-/-}$ mice developed pancreatitis after cerulein administration (Supplementary Figure 2). In addition, we eliminated the possibility that NK cells are involved in this model by showing that pre-administration of an anti-asialo GM1 monoclonal antibody did not affect the severity of the pancreatitis (Supplementary Figure 2). Overall, our data led to the conclusion that NK, NKT, and TCR$\gamma\delta^+$ T cells might not participate in the early stage of the pathogenesis of this model.

Therefore, it was interesting that the pancreatic CD11b^{high}CD11c^{-} population, which was absent under steady-state conditions, emerged in cerulein-injected mice at the highest ratio among the immune cells in the damaged pancreas. The marked increase in this population at 8 hours after cerulein administration suggests that this population migrated from outside of the pancreas, rather than expanding within the pancreas from precursors. This notion was supported by the findings that the resident macrophages under steady-state conditions were in the Gr-1^{-} subpopulation (S1), whereas the migratory macrophages during the inflammation were in the Gr-1^{low} subpopulation (S2) (Figure 1). In addition, cerulein-administered RAG-2$^{-/-}$ mice developed mild pancreatitis with a marked increase in the S2 macrophage subpopulation without the presence of T cells (Supplementary Figure 1).

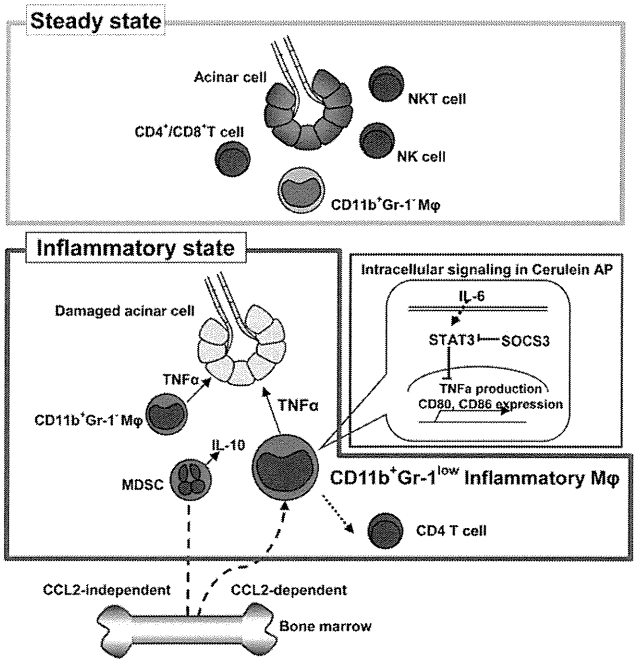

Figure 6. Two steps are required for development of cerulein-induced acute pancreatitis. Almost all sets of immune compartments, except for the CD11b^{high}CD11c^{-} population, reside in the pancreas under steady-state conditions (*upper, green*). During cerulein hyperstimulation (*lower, red*), the damaged acinar cells lead to CD11b^{high}Gr-1^{low} inflammatory macrophage migration into the pancreas in a CCL2-CCR2–dependent manner (step 1). Next, inflammatory macrophages are activated to produce TNF-α in a SOCS3-dependent manner (step 2). Finally, pancreatogenic CD4^{+} T cells interacted with the inflammatory macrophages establish the model. In contrast, granulocytes and IL-10–producing MDSCs migrate to the damaged pancreas in a CCL2-CCR2–independent manner.

In support of this, we detected up-regulation of CD80 and CD86 expression on pancreatic macrophages even in cerulein-administered RAG-2$^{-/-}$ mice (Supplementary Figure 1), suggesting the involvement of innate immune cells at an early stage of this model. Despite speculation that interferon-γ produced by effector CD4^{+} T cells in the pancreas of cerulein-injected mice activates macrophages,[26] our results indicate that S2 and S3 macrophages/granulocytes/MDSCs are the initiators in this model, and acquired immune cells, particularly conventional CD4^{+} T cells, are the eventual effectors that establish the model, possibly through cross talk with activated macrophages/granulocytes and CD4^{+} T cells. The pancreas can be controlled by distinctive subpopulations of macrophages: resident CD11b^{high}Gr-1^{-} macrophages (S1) under steady-state conditions and migratory CD11b^{high}Gr-1^{low} macrophages (S2) during inflammation.

We further examined the characteristics of the CD11b^{high}Gr-1^{-} (S1), CD11b^{high}Gr-1^{low} (S2), and CD11b^{high}Gr-1^{high} (S3) subpopulations because it is possible that the S2 and S3 subpopulations can include granulocytes and/or MDSCs.[18] We found that the S2 subpopulation that emerged during inflammation comprised morphologically and phenotypically homogeneous F4/80^{+}CD11c^{-}Ly6C^{high}Ly6G^{-} macrophages. These migratory cells should be responsible for development of acute pancreatitis induced by cerulein injection, because they not only produced a huge amount of TNF-α, but were also significantly decreased in nondiseased CCL2$^{-/-}$ mice injected with cerulein. In contrast, the S3 subpopulation did not express F4/80, and was composed of 2 subpopulations: dominant granulocyte-like cells with a segmented nucleus and minor macrophage-like cells with a horseshoe-shaped nucleus. Interestingly, the migration of the S3 subpopulation was not affected in nondiseased CCL2$^{-/-}$ mice injected with cerulein, suggesting that the migration of S3 cells is not mediated by the CCR2/CCL2 axis. Furthermore, in sharp contrast to the TNF-α–expressing S2 subpopulation, approximately half of the S3 subpopulation expressed IL-10 but not TNF-α. Although we did not determine which S3 subpopulations produced IL-10 during inflammation of the pancreas, inflammatory TNF-α–expressing S2 cells and protective IL-10-expressing S3 cells (possibly MDSCs) may migrate to the damaged pancreas via a distinct migratory pathway.

Our parabiosis experiments led to the particularly important conclusion that pathological monocytes, which migrate to the pancreas and become activated TNF-α–producing macrophages, are not derived from constantly circulating monocytes, but from a certain reservoir of monocytes. The surprising finding was that when cerulein was injected into one parabiont and PBS was injected into the partner, only mice injected with cerulein developed pancreatitis. These findings indicate that intraperitoneally injected cerulein directly affected the pancreas only in the injected animal, and monocytes in a certain reservoir of only the diseased mice, which were not constantly circulating monocytes, were only recruited to the damaged pancreas, in which CCL2 expression is up-regulated,[21] because the chimerism of macrophages in cerulein-injected mice should reach around 50% if constantly circulating mixed monocytes are recruited to the damaged pancreas. In this regard, we found that the absolute cell number of CD11b^{high}Gr-1^{low}Ly6C^{high} cells corresponding to the S2 population in the BM of mice injected with cerulein was significantly lower than that in PBS-injected mice, indicating that such cells are mobilized to the damaged pancreas from the BM.

After the migration of monocytes into the cerulein-induced damaged pancreas, the question arose as to which mechanisms of monocyte activation and differentiation to pathological macrophages operate in this model. To address this, we tested the possibility that SOCS3 plays a crucial role in the activation of pancreatic macrophages in this model. Consistent with this, it is known that both SOCS1 and SOCS3 participate in Toll-like receptor (TLR)/NF-κB signaling in macrophages. Unlike the SOCS1 signaling pathway, SOCS3 is a key regulator that suppresses IL-6–mediated STAT3 activation. Because STAT3 activation results in suppression of TLR/NF-κB signaling in macrophages, the lack of the SOCS3 signaling pathway can accelerate the STAT3 activation, resulting in the amelioration of pancreatitis in this model (Figure 6). Additional studies will be needed to determine which kinds of endogenous ligands stimulate

TLR/NF-κB signaling and activate SOCS3 in macrophages in the pathogenesis of acute pancreatitis.

Finally, we tested another model of acute pancreatitis, the L-Arg model, to determine a general concept for the pathogenesis of murine acute pancreatitis. We found not only that $CD11b^{+}CD11c^{-}Gr-1^{low}$ S2 macrophages showed a marked increase in the inflamed pancreas of this second model, but also that $CCL2^{-/-}$ mice were resistant to this model in accordance with the cerulein model. However, unlike the cerulein model, we did not detect statistically significant differences between L-Arg-injected WT mice and SOCS3cKO mice, suggesting that SOCS3 was not strongly involved in S2 macrophage activation in this model, although L-Arg-injected WT mice tended to develop mild pancreatitis. Therefore, CCL2/CCR2-dependent migratory macrophages are essential for the pathogenesis of acute pancreatitis, but the activation process of macrophages in the damaged pancreas occurs in a model-dependent manner.

In summary, the following consecutive immunological events are required for the development of cerulein-induced acute pancreatitis: CCL2/CCR2-dependent $CD11b^{high}CD11c^{-}Gr\text{-}1^{low}Ly6C^{high}$ monocyte/macrophage migration from the BM and SOCS3-dependent macrophage activation. These findings provide a new concept for therapeutic strategies against acute pancreatitis.

Supplementary Material

Note: To access the supplementary material accompanying this article, visit the online version of *Gastroenterology* at www.gastrojournal.org, and at doi: 10.1053/j.gastro.2008.07.064.

References

1. Baron TH, Morgan DE. Acute necrotizing pancreatitis. N Engl J Med 1999;340:1412–1417.
2. Sand J, Nordback I. Acute pancreatitis: risk of recurrence and late consequences of the disease. Nat Rev Gastroenterol Hepatol 2009;6:470–477.
3. Saluja AK, Lerch MM, Phillips PA, et al. Why does pancreatic overstimulation cause pancreatitis? Annu Rev Physiol 2007;69:249–269.
4. Hashimoto D, Ohmuraya M, Yamamura K, et al. Involvement of autophagy in trypsinogen activation within the pancreatic acinar cells. J Cell Biol 2008;181:1065–1072.
5. Mareninova OA, Hermann K, Gukovskaya AS, et al. Impaired autophagic flux mediates acinar cell vacuole formation and trypsinogen activation in rodent models of acute pancreatitis. J Clin Invest 2009;119:3340–3355.
6. Yang CY, Chang-Chien CS, Liaw YF. Controlled trial of protease inhibitor gabexelate mesilate (FOY) in the treatment of acute pancreatitis. Pancreas 1987;2:698–700.
7. Büchler M, Malfertheiner P, Beger HG, et al. Gabexate mesilate in human acute pancreatitis. German Pancreatitis Study Group. Gastroenterology 1993;104:1165–1170.
8. Chen HM, Chen JC, Hwang TL, et al. Prospective and randomized study of gabexate mesilate for the treatment of severe acute pancreatitis with organ dysfunction. Hepatogastroenterology 2000;47:1147–1150.
9. de Beaux AC, Palmer KR, Carter DC. Factors influencing morbidity and mortality in acute pancreatitis; an analysis of 279 cases. Gut 1995;37:121–126.
10. Kylänpää ML, Repo H, Puolakkainen PA. Inflammation and immunosuppression in severe acute pancreatitis. World J Gastroenterol 2010;16:2867–2872.
11. Sakai Y, Masamune A, Shimosegawa T, et al. Macrophage migration inhibitory factor is a critical mediator of severe acute pancreatitis. Gastroenterology 2003;124:725–736.
12. Sandoval D, Gukovskaya A, Pandol SJ, et al. The role of neutrophils and platelet-activating factor in mediating experimental pancreatitis. Gastroenterology. 1996;111:1081–1091.
13. Demols A, Le Moine O, Desalle F, et al. $CD4^{+}$ T cells play an important role in acute experimental pancreatitis in mice. Gastroenterology 2000;118:582–590.
14. Grady T, Liang P, Logsdon CD. Chemokine gene expression in rat pancreatic acinar cells is an early event associated with acute pancreatitis. Gastroenterology 1997;113:1966–1975.
15. Pandol SJ, Saluja AK, Imrie CW, et al. Acute pancreatitis: bench to the bedside. Gastroenterology 2007;132:1127–1151.
16. Chan YC, Leung PS. Acute pancreatitis: animal models and recent advances in basic research. Pancreas 2007;34:1–14.
17. Domínguez PM, Ardavín C. Differentiation and function of mouse monocyte-derived dendritic cells in steady state and inflammation. Immunol Rev 2010;234:90–104.
18. Gabrilovich DI, Nagaraj S. Myeloid-derived suppressor cells as regulators of the immune system. Nat Rev Immunol 2009;9:162–174.
19. Serbina NV, Jia T, Hohl, et al. TM, Monocyte-mediated defense against microbial pathogens. Annu Rev Immunol 2008;26:421–452.
20. Zhang Y, Rollins BJ. A dominant negative inhibitor indicates that monocyte chemoattractant protein 1 functions as a dimer. Mol Cell Biol 1995;15:4851–4855.
21. Bhatia M, Ramnath RD, Chevali L, et al. Treatment with bindarit, a blocker of MCP-1 synthesis, protects mice against acute pancreatitis. Am J Physiol Gastrointest Liver Physiol 2005;288:1259–1265.
22. Geissmann F, Manz MG, Jung S, et al. Development of monocytes, macrophages, and dendritic cells. Science 2010;327:656–661.
23. Cuzzocrea S, Mazzon E, Thiemermann C, et al. Absence of endogenous interleukin-6 enhances the inflammatory response during acute pancreatitis induced by cerulein in mice. Cytokine 2002;18:274–285.
24. Yoshimura A, Naka T, Kubo M. SOCS proteins, cytokine signaling and immune regulation. Nat Rev Immunol 2007;7:454–465.
25. Hegyi P, Rakonczay Z Jr, Sári R, et al. L-arginine-induced experimental pancreatitis. World J Gastroenterol 2004;10:2003–2009.
26. Hayashi T, Ishida Y, Kimura A, et al. IFN-gamma protects cerulein-induced acute pancreatitis by repressing NF-kappa B activation. J Immunol 2007;178:7385–7394.

Received November 25, 2010. Accepted December 9, 2011.

Reprint requests

Address requests for reprints to: Toshifumi Hibi, MD, PhD, Division of Gastroenterology and Hepatology, Department of Internal Medicine, Keio University School of Medicine, Tokyo 180-8582, Japan. e-mail: thibi@sc.itc.keio.ac.jp; Fax: +81-3-3341-3631.

Conflicts of interest

The authors disclose no conflicts.

Funding

This study was supported in part by Grants-in-Aid for Scientific Research, Scientific Research on Priority Areas, Exploratory Research and Creative Scientific Research from the Japanese Ministry of Education, Culture, Sports, Science and Technology; by the Research Fund of Yakult Medical Foundation; and by the Keio University Medical Fund.

Supplementary Materials and Methods

Mice

C57BL/6 mice were purchased from Japan CLEA (Tokyo, Japan). C57BL/6-Ly5.1 and C57BL/6-RAG-2$^{-/-}$ mice were obtained from Taconic Laboratory (Hudson, NY) and Central Laboratories for Experimental Animals (Kawasaki, Japan). Macrophage chemoattractant protein 1 knockout (MCP-1$^{-/-}$ [also known as CCL2$^{-/-}$]) mice[1] and LTa$^{-/-}$ mice[2] were purchased from Jackson Laboratories (Bar Harbor, ME). Interleukin-23 p19 knockout (IL-23p19$^{-/-}$) mice,[3] γδT cell receptor knockout (TCR γδ$^{-/-}$) mice,[4] lysozyme M (LysM)-Cre/Socs1$^{flox/flox}$ conditional knockout (cKO) mice, and LysM-Cre/Socs3$^{flox/flox}$ cKO mice were previously generated by one of the authors (A. Yoshimura).[5] CD1d$^{-/-}$ mice were previously generated by S.K. Mendiratta.[6] All mice had the C57BL/6 background and were housed in our specific pathogen-free animal facility. All experiments were approved by the regional animal study committees and performed according to the guidelines of the animal ethics committee of Keio University, Tokyo, Japan.

Induction of Acute Pancreatitis

Cerulein (Sigma-Aldrich, St. Louis, MO) was dissolved with phosphate-buffered saline (PBS) (Wako, Osaka, Japan) and administered intraperitoneally at a dose of 50μg/kg at intervals of 1 h (total of 8 injections). In some experiments using parabionts (Figure 3, Group 3), cerulein was administered unilaterally at a dose of 100μg/kg. The mice were euthanized by cervical dislocation at 1 h after the last cerulein injection. Before euthanasia, whole blood was collected from the ocular artery under light ether anesthesia. After euthanasia, the pancreas and spleen were excised and immediately weighed. For histological analysis, the pancreas was fixed in 10% formaldehyde (Wako) for H&E staining. For L-Arginine-induced Acute Pancreatitis, L-Arginine monohydrochloride (Sigma-Aldrich) was dissolved in saline and administered intraperitoneally in two doses of 4 g/kg spaced 1 h apart and mice were euthanized at 72 h later as previously described.[7]

Histological Score

Microscopic images were taken under a light microscope (Nikon, Tokyo, Japan) using ACT software (Nikon). Histological scoring was performed using a point-counting morphometry method as described previously.[8] Briefly, a 10 × 10-μm grid was superimposed on three randomly-chosen microscopic images of every section, and the interstitial space under each grid point was counted.

Serum Amylase and Lipase Levels

Sera were diluted 5-fold with pure water and stored at −80°C until analysis. The amylase and lipase levels were analyzed according to standard procedures.

Mononuclear Cell Isolation

For mononuclear cell isolation, the pancreas was minced and digested with 3 mg/ml collagenase A (Roche, Mannheim, Germany) for 15 min. The digest was filtered through a 40-μm cell strainer and washed with 1.5% FCS-containing Hank's balanced salt solution. Next, the suspended cells were centrifuged at 50 × *g* for 30 s to eliminate the major debris. The total mononuclear cells were further purified by 40–70% Percoll gradient centrifugation. Splenic mononuclear cells were isolated by mechanical homogenization. Bone marrow cells were isolated from the femur.

Flow Cytometry Analysis

Isolated cells were incubated with an anti-CD16/CD32 antibody (BD Pharmingen, Tokyo, Japan) to prevent non-specific antibody binding.[9] Surface antigens were stained with the following antibodies conjugated with fluorescein isothiocyanate (FITC), phycoerythrin (PE), allophycocyanin (APC), phycoerythrin-Cy7 (PECy7), or allophycocyanin-Cy7 (APCCy7): CD3e-FITC, CD3e-APCCy7, CD4-PE, CD4-PECy7, CD8α-APCCy7, NK1.1-APC, γδTCR-FITC, CD11b-PECy7, CD11c-APC, Ly6G and Ly6C-APCCy7 (Gr-1, clone: RB6-8C5), Ly6G-PE (clone: 1A8), Ly5.2-FITC, CD49b-FITC (clone: DX5), CD80-PE, CD86-PE, Ly6C-FITC, and B220-FITC. The corresponding isotype IgGs were obtained from BD Pharmingen. F4/80-APC was obtained from eBioscience. Dead cells were eliminated by 7-AAD (BD Pharmingen) according to the manufacturer's protocol. Flow cytometry was performed with a FACSCanto II and cell sorting was performed with a FACSAria (both from BD Biosciences, San Jose, CA). All data were re-analyzed with FlowJo Version 7.2.5 software (TreeStar, Ashland, OR). The mean fluorescence intensity (MFI) was calculated as follows: MFI = (CD80 or CD86 geometric mean) − (isotype geometric mean).

Cell Counts

Isolated cells were counted under a light microscope. To avoid counting dead cells, cells were incubated with Gibco Trypan Blue Stain 0.4% (Invitrogen, Carlsbad, CA). The absolute cell number of mononuclear cells in the pancreas was estimated as follows: Total cell count = (isolated cell count) × (total wet weight)/(wet weight used for cell isolation). The cell number in each leukocyte subset was calculated by regarding the 7-AAD^{-}/characteristic FSC, SSC-gated monocyte subset as counted cells.

Parabiosis

Surgical gloves and autoclaved sterilized instruments were used. Sodium pentobarbital was administered intraperitoneally for sedation. After shaving the corresponding lateral aspects of each mouse, matching skin incisions were made from the base of the anterior to posterior extremities of each mouse, and the subcutane-

ous fascia was bluntly dissected to create about 1/2 cm of free skin. The parabionts were then combined by suturing the corresponding free skin densely with surgical clips.[10] The percent chimerism was defined for gated monocytes as % CD45.1$^+$ cells/Ly5.1$^+$ + Ly5.2$^+$ cells in Ly5.2 mice and as % Ly5.2 cells/Ly5.1$^+$ + Ly5.2$^+$ cells in Ly5.1 mice in the indicated cells. In some experiments, parabiosis surgery was performed between Ly5.1$^+$ WT and Ly5.2$^+$ CCL2$^{-/-}$ mice, and both mice were injected with cerulein (50 μg/kg for each mouse) at 2 wk after the surgery (Supplementary Figure 6*A*).

Intracellular Cytokine Staining

Isolated cells were cultured with or without 1 μg/ml of lipopolysaccharide (LPS) in 10% FCS-containing RPMI1640 medium for 5 h. After surface staining with CD11b-PECy7, Ly6G and Ly6C-APCCy7, and CD3e-PerCPCy5.5 antibodies, the cells were fixed and permeabilized with a Cytofix/Cytoperm Kit (BD Biosciences) according to the manufacturer's protocol. For cytokine staining, IL-10-APC and TNFα-PE antibodies (BD Pharmingen) were used.

Phosphorylation of Transcription Factors

Total collagenase-digested cells were harvested for phosphorylation analyses of p38 MAPK and STAT3 using the phosflow method (BD Pharmingen) according to the manufacturer's instructions. For flow cytometry staining, F4/80-FITC, STAT3 (pY705)-PE, and p38MAPK-PE antibodies (BD Pharmingen) were used.

NK Cell Depletion

Selective depletion of NK cells was achieved with a rabbit anti-asialoGM1 monoclonal antibody (250 μg intraperitoneal; Wako) at 24 h and 72 h before the first cerulein injection. Control mice were injected with nonspecific IgG (Sigma-Aldrich) using the same regimen. Pancreatic and splenic NK cell depletion was confirmed by flow tometry (data not shown).

Acinar Cell Isolation and Cytotoxicity Assay

Acinar cells were isolated from the normal pancreas as previously described with some modifications.[12] Briefly, collagenase A solution (0.18 mg/ml) was injected into the pancreas and thereafter the tissue was digested for 30 min. The digest tissue was further broken up to single acinar cells or acini by pipetting and washed with 4% BSA-containing RPMI1640 medium. The viability was confirmed >95% and the purity was >99% by flow cytometry with the staining of 7-AAD and anti-CD45.2 Ab. Acinar cells were cultured in 10%FCS-containing RPMI1640 for 5 h with or without FACSAria-sorted S2 macrophages, S3 granulocytes, and a hamster anti-mouse TNF-α antibody (clone: TN3-19.12; BioLegend, San Diego, CA) on 48-well plates. Apoptotic and dead acinar cells were evaluated by flow cytometry after staining with annexin V (BD Pharmingen) and 7-AAD according to the manufacturer's protocol.

Cytokine Bead Assay

Cytokine bead assays were performed using a mouse Th1/Th2/Th17 CBA Kit (BD Biosciences) according to the manufacturer's protocol.

Macrophage Depletion

Macrophages were depleted by intraperitoneal injection of Clodronate Liposomes (50 mg/kg; Encapsula Nanosciences, Nashville, TN) at 24 h before the first injection of cerulein. For control mice, Plain Liposomes (Encapsula Nanosciences) were injected. Macrophage depletion was confirmed by flow cytometry of splenic macrophages (data not shown).

Quantitative RT-PCR

Total RNA was extracted from FACSAria-sorted CD11b$^+$ macrophages using the TRIzol reagent (Invitrogen) according to the manufacturer's protocol. SOCS1 (Mm00782550_s1) and SOCS3 (Mm00545913_s1) mRNA expression was assessed by real-time PCR using a TaqMan Gene Expression Assays Kit (Applied Biosystems, Foster City, CA) according to the manufacturer's protocol. Briefly, 1 μg of total RNA was reverse-transcribed to cDNA using TaqMan Universal Master Mix and quantitative PCR was performed using a StepOnePlus\™\System (Applied Biosystems) and TaqMan technology. Data were analyzed using the DCT method, and the expression levels were normalized by the expression of b-actin as an internal control.

Statistical Analysis

The Mann-Whitney U test was used for statistical analysis of the histological scores, and an unpaired Student's *t* test was used for other analyses. All analyses were performed with JMP software version 7.0 (SAS Institute Inc., Cary, NC), and values of $P < 0.05$ were considered to indicate statistical significance. All graphs were drawn using GraphPad Prism 5 for Windows software (GraphPad Software Inc., San Diego, CA), and all data were presented as means ± SEM.

Supplemental References

1. Lu B, Rutledge BJ, Gu L, et al. Abnormalities in monocyte recruitment and cytokine expression in monocyte chemoattractant protein 1-deficient mice. J Exp Med. 1998;187:601–8.
2. De Togni P, J Goellner, NH Ruddle, et al. Abnormal development of peripheral lymphoid organs in mice deficient in Lymphotoxin. Science. 1994;264:703–707.
3. Cua DJ, Sherlock J, Chen Y, et al. Interleukin-23 rather than interleukin-12 is the critical cytokine for autoimmune inflammation of the brain. Nature. 2003; 421: 744–748.
4. Shichita T, Sugiyama Y, Ooboshi H, et al. Pivotal role of cerebral interleukin-17-producing gammadeltaT cells in the delayed phase of ischemic brain injury. Nat Med 2009;15:946–50.

5. Yasukawa H, Ohishi M, Mori H, et al. IL-6 induces an anti-inflammatory response in the absence of SOCS3 in macrophages. Nat Immunol 2003;4:551–6.
6. Mendiratta SK, Martin WD, Hong S, et al. CD1d1 mutant mice are deficient in natural T cells that promptly produce IL-4. Immunity. 1997;6:469–477.
7. Dawra R, Sharif R, Saluja AK. et al. Development of a new mouse model of acute pancreatitis induced by administration of L-arginine. Am J Physiol Gastrointest Liver Physiol. 2007;292:1009–18.
8. Barreto SG, Carati CJ, Saccone GT. et al. The combination of neurokinin-1 and galanin receptor antagonists ameliorates caerulein-induced acute pancreatitis in mice. Peptides. 2010; 31:315–321.
9. Mikami Y, Kanai T, Sujino T, et al. Competition between colitogenic Th1 and Th17 cells contributes to the amelioration of colitis. Eur J Immunol 2010;40:2409–22.
10. Tomita T, Kanai T, Nemoto Y, et al. Systemic, but not intestinal, IL-7 is essential for the persistence of chronic colitis. J Immunol 2008; 180: 383–90.
11. Nakamura Y, Do JH, Pandol SJ, et al. Inflammatory cells regulate p53 and caspases in acute pancreatitis. Am J Physiol Gastrointest Liver Physiol. 2010;298:92–100.

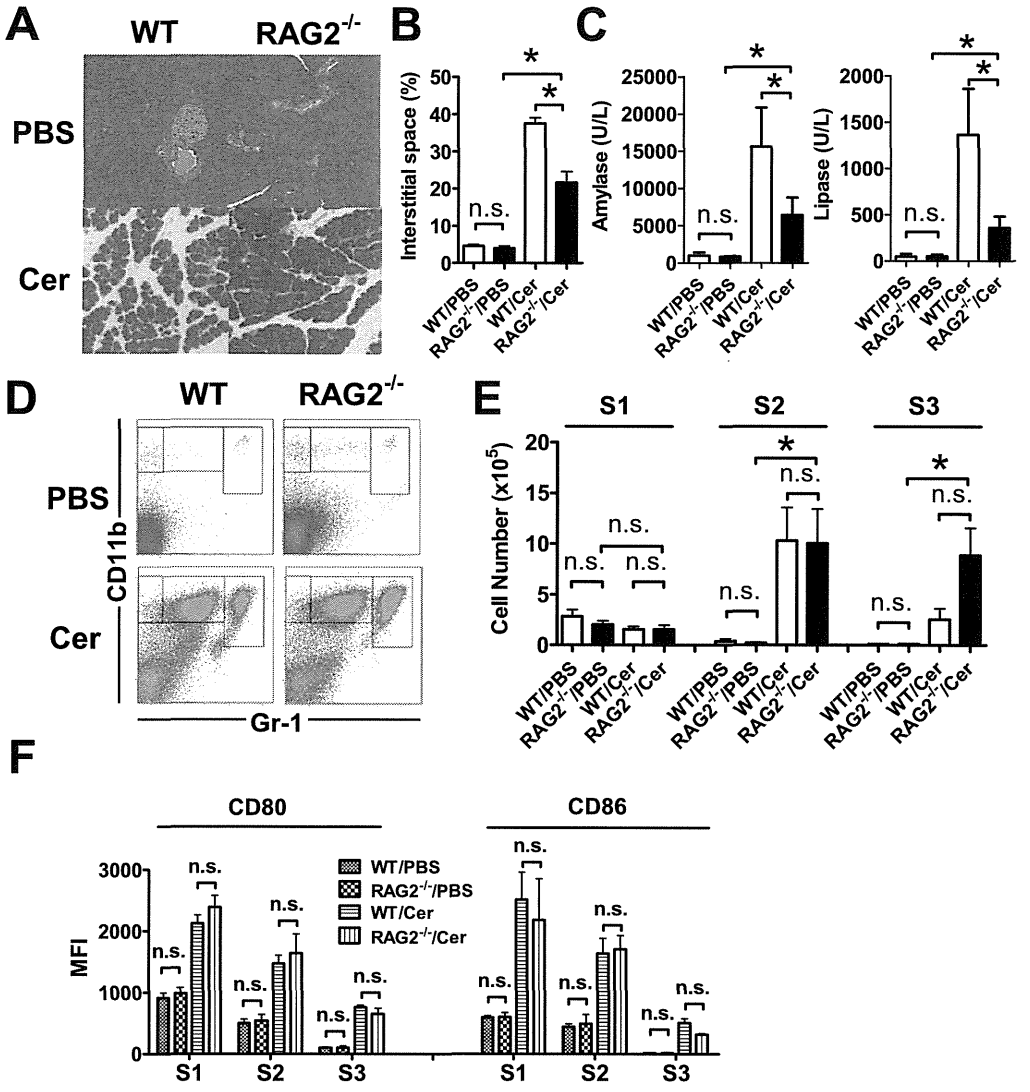

Supplementary Figure 1. Cerulein-administered RAG2$^{-/-}$ mice develop mild pancreatitis. (*A*) H&E staining of the pancreas of cerulein- or PBS-administered WT or RAG-2$^{-/-}$ mice. Original magnification, ×200. (*B*) Histological scores ($n = 6$). *$P < .05$; n.s., not significant. (*C*) Serum amylase and lipase levels ($n = 10$). *$P < .05$; n.s., not significant. (*D*) Expression of CD11b/Gr-1 on pancreatic cells of the indicated mice administered cerulein. (*E*) Absolute cell numbers of each subpopulation ($n = 4$) of the indicated mice administered cerulein or PBS. *$P < .05$; n.s., not significant. (*F*) Mean fluorescence intensities of CD80 and CD86 on each subpopulation ($n = 4$) of the indicated mice administered cerulein or PBS. Data are representative of two independent experiments. n.s., not significant. *Cer;* cerulein.

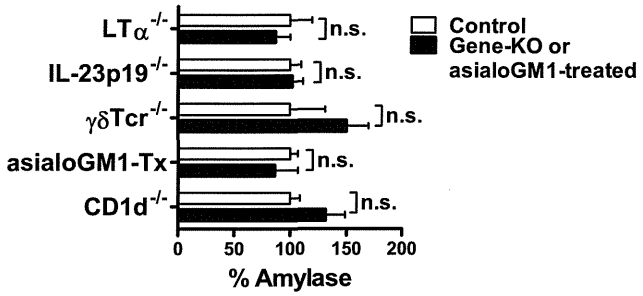

Supplementary Figure 2. Induction of pancreatitis by cerulein administration in various gene-deficient mice and anti-asialoGM1 monoclonal antibody-treated mice. LTa$^{-/-}$ mice and littermate controls (n = 5 each), IL-23p19$^{-/-}$ mice and littermate controls (n = 13 each), CD1d$^{-/-}$ mice and littermate controls (n = 7 each), gdTcr$^{-/-}$ mice and littermate controls (n = 4 each), and anti-asialoGM1 mAb- or isotype-matched monoclonal antibody-treated mice (n = 5 each) were administered cerulein at intervals of 1 h (total of 8 injections). The serum amylase levels were measured and %amylase was calculated as follows: (serum amylase level of each individual)/(mean amylase level of control).

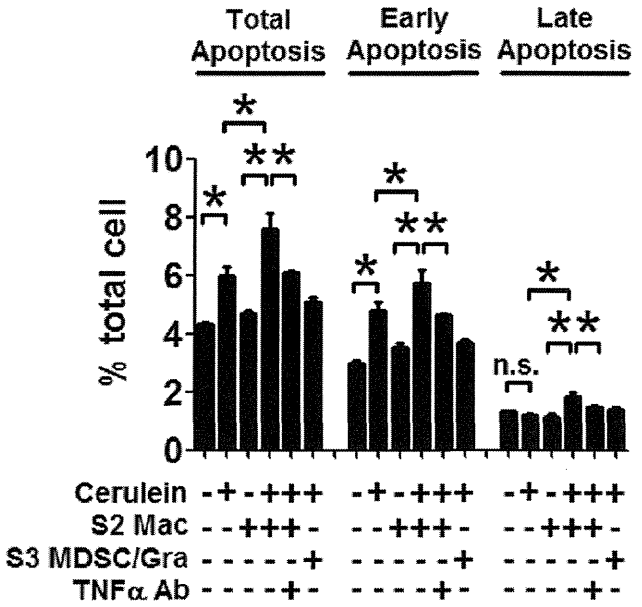

Supplementary Figure 4. S2 macrophage-derived TNF-α regulates acinar cell apoptosis. Acinar cells were cultured for 5 h with or without 10 nM cerulein, with or without 1 × 10^5 S2 macrophages or S3 granulocytes (Gra)/MDSCs, and with or without 1 μg of an anti-TNF-α antibody. The viability of the cultured acinar cells was evaluated by flow cytometry after annexin V/7-AAD staining. Early apoptosis was defined as the annexin V$^+$/7-AAD$^-$ subpopulation and late apoptosis was defined as the annexin V$^+$/7-AAD$^+$ subpopulation of the total cells (n = 6/each group).

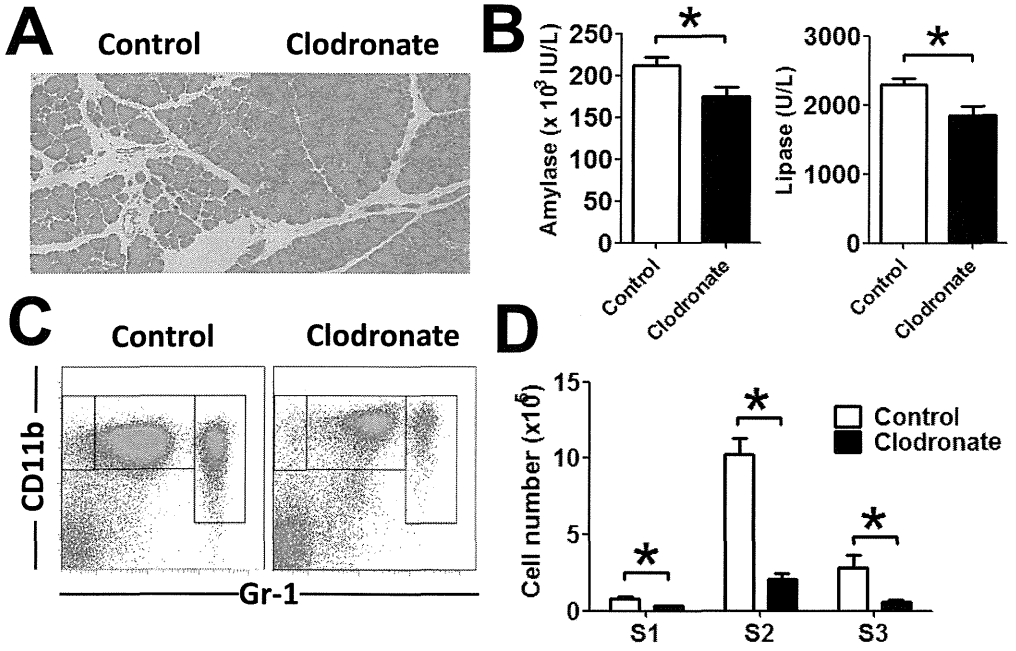

Supplementary Figure 3. Macrophage depletion reduces the severity of cerulein-induced acute pancreatitis. Macrophages were depleted by injection of Clodronate Liposomes at 24 h before cerulein administration. (*A*) H&E staining of the pancreas of the indicated cerulein-administered mice. Original magnification, ×200. (*B*) Serum amylase and lipase levels (n = 5). *P < .05; n.s., not significant. (*C*) Expression of CD11b/Gr-1 on pancreatic cells of the indicated mice administered cerulein. (*D*) Absolute cell numbers of each subpopulation (n = 5) of the indicated mice. Data are representative of two independent experiments. *P < .05.

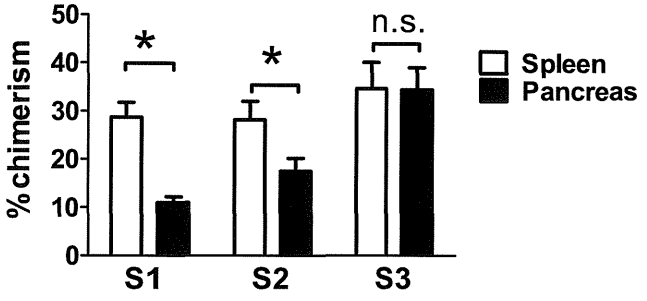

Supplementary Figure 5. Hemodynamics of pancreatic mononuclear cells. Parabiosis surgery was performed as depicted in Figure 4*A*. The percentages of chimerism of the pancreatic and splenic S1, S2, and S3 subpopulations were determined by using non-treated parabionts at 5 wk after the operation (n = 4).

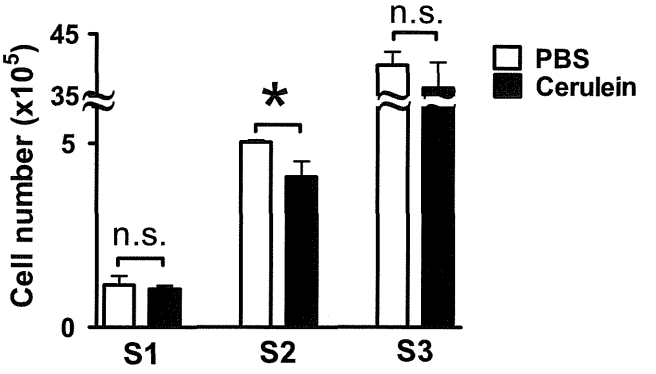

Supplementary Figure 7. BM is a reservoir for CD11b^{high}Gr-1^{low}Ly6C^{high} S2 macrophages in the development of cerulein-induced pancreatitis. The absolute cell numbers of each BM cell subpopulation in cerulein- or PBS-administered mice (n = 4) are shown. Each mouse was injected intraperitoneally at intervals of 1 h (total of 8 injections), and euthanized at 1 h after the last injection. *P < .05; n.s., not significant.

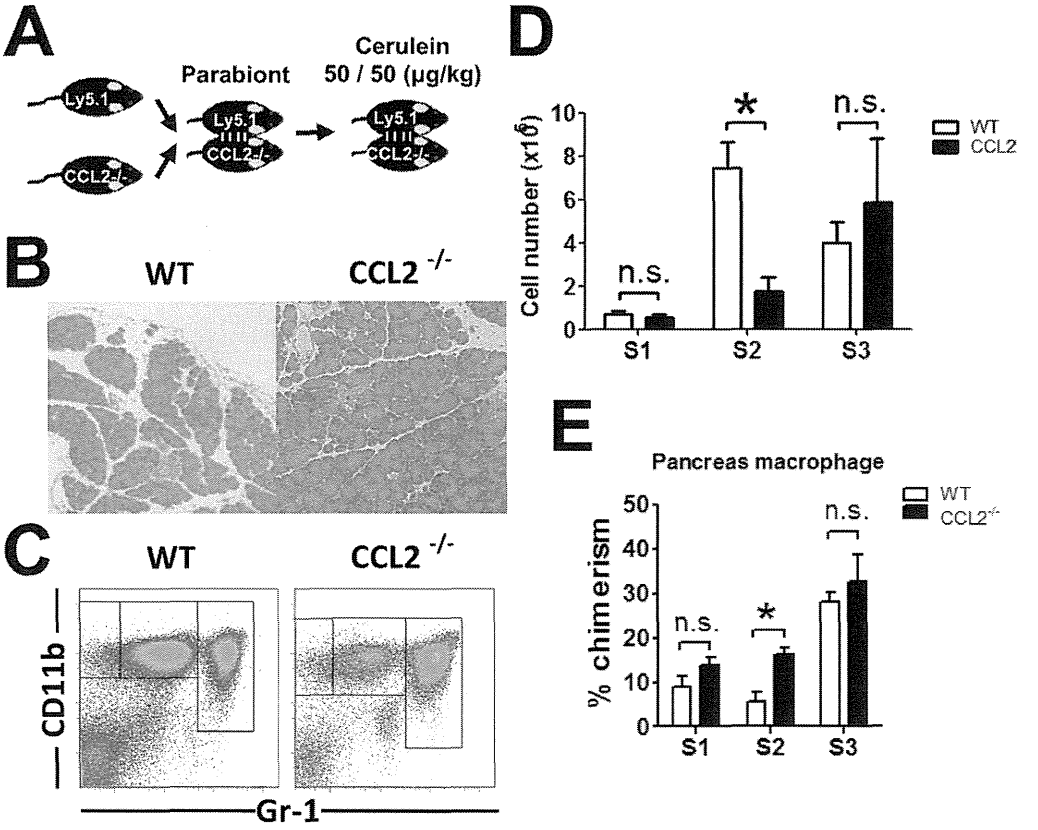

Supplementary Figure 6. Pancreatic S2 macrophages are recruited from the host reservoir in both WT and CCL2$^{-/-}$ mice. (*A*) Study design. Parabionts of Ly5.1-WT mice combined with Ly5.2-CCL2$^{-/-}$ mice were administered 50 μg/kg of cerulein bilaterally at 2 wk after the operation. (*B*) H&E staining of the pancreas. Original magnification, ×200. (*C*) Flow cytometry of CD11b/Gr-1 and (*D*) absolute cell numbers of each subpopulation (n = 4). *P < 0.05; n.s., not significant. (*E*) Percentages of chimerism of each subpopulation (n = 4). *P < .05; n.s., not significant.

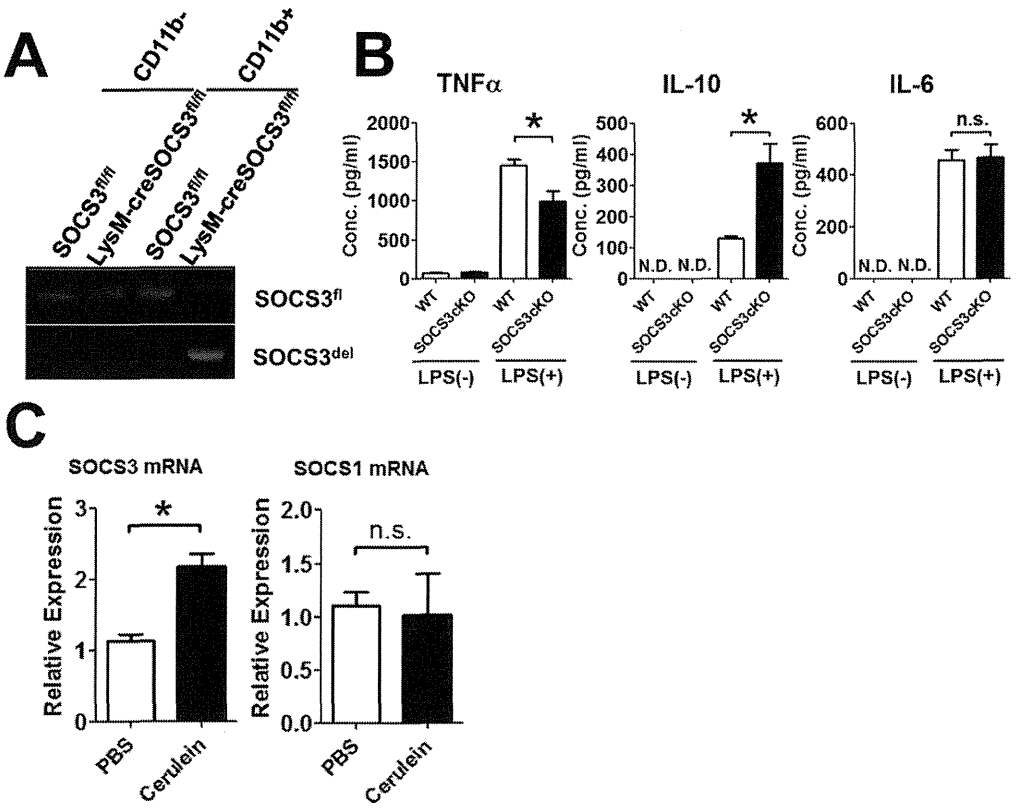

Supplementary Figure 8. SOCS3 is upregulated during cerulein-induced acute pancreatitis. (*A*) SOCS3 is deleted in CD11b$^+$ pancreatic macrophages. Data are representative of three independent experiments. (*B*) LPS-mediated secretion of proinflammatory cytokines in splenic CD11b$^+$ macrophages ($n = 4$). In the presence of 1 μg/ml LPS, 1×10^5 splenic WT or SOCS3-deficient CD11b$^+$ macrophages were cultured for 24 h with 10% FCS-containing RPMI1640 medium on 96-well round-bottom plates. Cytokine secretion was analyzed by cytokine bead assays. (*C*) SOCS3, but not SOCS1, mRNA is upregulated in pancreatic CD11b$^+$ macrophages during cerulein-induced acute pancreatitis ($n = 3$). Data are representative of two independent experiments.

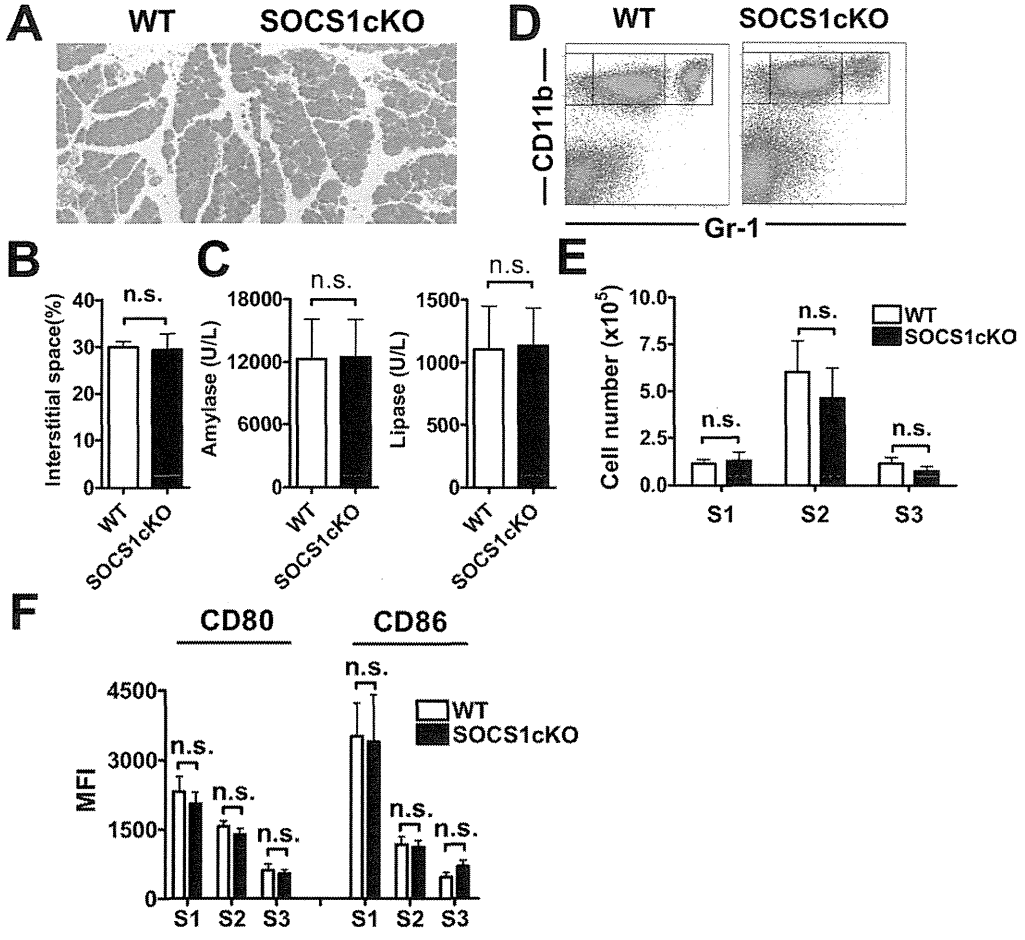

Supplementary Figure 9. SOCS1 in macrophages does not affect the severity of cerulein-induced pancreatitis. (*A*) H&E staining of the pancreas in cerulein-administered mice. Original magnification, ×200. (*B*) Histological scores ($n = 3$). (*C*) Serum amylase and lipase levels ($n = 3$). (*D*) Expression of CD11b/Gr-1. (*E*) Absolute cell numbers of each pancreatic subpopulation ($n = 3$). n.s., not significant. (*F*) Mean fluorescence intensities of CD80 and CD86 on pancreatic cells ($n = 3$). n.s., not significant.

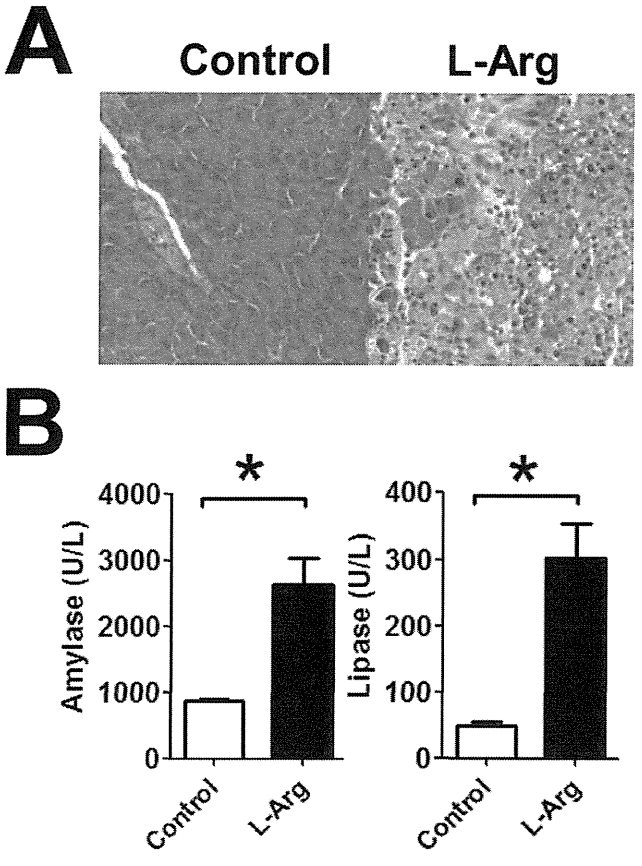

Supplementary Figure 10. L-Arginine-induced acute pancreatitis. Acute pancreatitis was induced by two sequential administrations of L-Arginine. (*A*) H&E staining of the pancreas of L-Arginine- or saline-administered mice. Original magnification, ×200. (*B*) Serum amylase and lipase levels ($n = 4$). *$P < .05$. Data are representative of four independent experiments. *L-Arg;* L-Arginine.

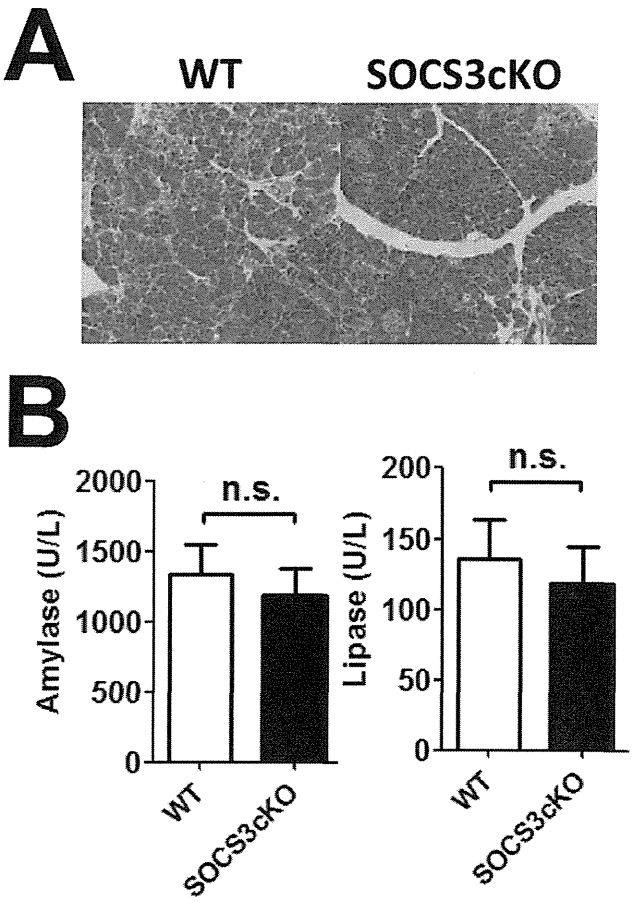

Supplementary Figure 11. SOCS3 in macrophages does not regulate the severity of L-Arginine-induced acute pancreatitis. (*A*) H&E staining of the pancreas in L-Arginine-administered mice. Original magnification, ×200. (*B*) Serum amylase and lipase levels ($n = 17$). Data were pooled from three independent experiments. n.s., not significant.

Phenotypic changes of lymphocyte in a patient with IgG4-related disease after corticosteroid therapy

Immunoglobulin G4-related disease (IgG4RD) is a novel clinical disease entity characterised by elevated serum IgG4 and tissue infiltration by IgG4-positive plasma cells.[1 2] Interleukin 4 (IL-4) and IL-10, which were detected with B cells in the salivary gland in this disease,[3] direct naive B cells to switch to IgG4 production.[4] B cells are therefore considered to be important for the pathogenesis of IgG4RD. However, the phenotype of B cells in patients with IgG4RD remains elusive. In this report we show the phenotypic changes of peripheral blood B cells in a patient with IgG4RD analysed by flow cytometry during treatment with a corticosteroid.

In January 2011 a 53-year-old man presented with symmetrical swelling of the lachrymal glands and a tumour located in the left junction of the renal pelvis and ureter, serum IgG4 >135 mg/dl and IgG4+/IgG+ cells >40% with significant invasion of lymphocytes and plasma cells, typical tissue fibrosis and sclerosis in the salivary gland. He was diagnosed with IgG4RD based on the guidelines for diagnosis.[5] Treatment with corticosteroid 40 mg (0.6 mg/kg) was started. One year later the bilateral renal pelvic tumour had disappeared and serum IgG (IgG4) decreased from 1692 (341) mg/dl to 969 (61.5) mg/dl despite tapering of the corticosteroid dose to 2 mg/day.

Meanwhile, before treatment, memory B cells (CD19 gated IgD-CD27 or CD27+ CD38-) and plasmablasts (CD19 gated $CD27^{high}CD38^{high}$ or IgD-$CD27^{high}$, $CD19^{low}CD38^{high}$) increased in a patient with IgG4RD compared with healthy donors in peripheral blood. Moreover, the expression levels of the costimulatory molecules CD80 were upregulated. Spleen tyrosine kinase (Syk) is a tyrosine kinase expressed in various immunocompetent cells including B cells. We have reported that the engagement of immune receptor phosphorylates Syk, resulting in proliferation and cytokine production on B cells.[6] It is noteworthy that Syk phosphorylation was also markedly increased in CD19 cells in the patient compared with those in healthy donors.

However, $CD27^{high}CD38^{high}$ plasmablasts in the patient decreased at 1 month and disappeared 6 months after treatment with corticosteroid, whereas the percentage of memory B cells almost did not change. Although he remained in low disease activity after tapering of the corticosteroid dose, the expression levels of CD80 and phospho-Syk on CD19 cells did not change until 1 year later (figure 1).

Taken together, although corticosteroid therapy effectively decreased peripheral plasmablasts, activated memory B cells were resistant to treatment in IgG4RD. These results are supported by those of Khosroshahi et al who demonstrated that B cell depletion therapy by rituximab was effective in some patients with IgG4RD refractory to corticosteroid.[7] The present data could therefore partly explain why IgG4RD is difficult to maintain in remission after reduction in the dose of corticosteroid. The results also indicate that the combined use of immunosuppressants, B cell-targeted therapies or Syk inhibitors may be considered for the treatment of IgG4RD, as shown in systemic lupus erythematosus, rheumatoid arthritis and idiopathic thrombocytopenic purpura.[8–10] However, further analysis of a large sample of patients is needed.

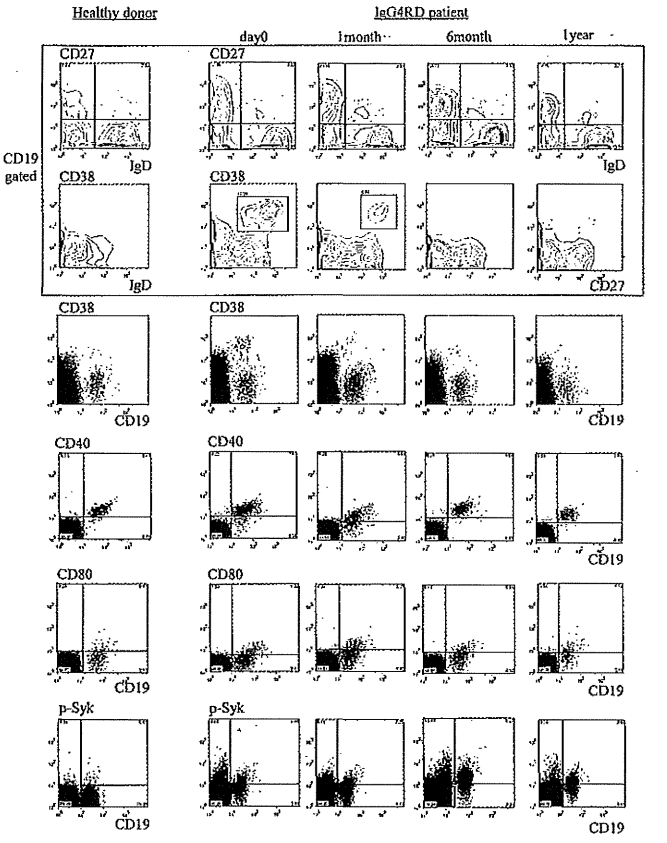

Figure 1 Phenotypic changes of B cells in a patient with IgG4-related disease before treatment, 1 month and 6 months after treatment with corticosteroid therapy. In the upper 10 contour line graphs, peripheral blood mononuclear cell (PBMCs) were gated on CD19-positive cells and further separated with CD27 and IgD, or CD38 and CD27. In the former, the left quadrant identified plasma cells (IgD-$CD27^{high}$) and class-switched memory B cells (IgD-CD27+). The right upper quadrant identified IgM memory B cells (IgD+CD27). The right lower quadrant identified naïve B cells (IgD+CD27+). In the latter, CD27−CD38 + identified naïve B cells, CD27+ CD38− identified memory B cells and $CD27^{high}CD38^{high}$ identified plasmablasts and plasma cells. In the lower four line graphs, PBMC were double-stained by CD19 (x-axis) and IgG isotype control, CD38, CD40, CD80 and Syk phosphorylation, respectively (y-axis). $CD19^{low}CD38^{high}$ identified plasmablasts and plasma cells.

Shigeru Iwata, Kazuyoshi Saito, Shintaro Hirata, Yoshiya Tanaka

The First Department of Internal Medicine, School of Medicine, University of Occupational and Environmental Health, Japan, Kitakyushu, Japan

Correspondence to Yoshiya Tanaka, University of Occupational and Environmental Health, Japan, The First Department of Internal Medicine, School of Medicine, 1-1 Iseigaoka, Yahatanishi Ward, Kitakyushu 807-8555, Fukuoka Prefecture, Japan; tanaka@med.uoeh-u.ac.jp

Acknowledgements The authors thank Ms T Adachi, Ms N Sakaguchi and Ms K Noda for the excellent technical assistance. This work was supported in part by a Research Grant-In-Aid for Scientific Research from the Ministry of Health, Labour and Welfare of Japan, the Ministry of Education, Culture, Sports, Science and Technology of Japan and the University of Occupational and Environmental Health, Japan.

Competing interests YT has received consulting fees, speaking fees and/or honoraria from Mitsubishi-Tanabe Pharma, Chugai Pharma, Eisai Pharma, Pfizer, Abbott Immunology Pharma, Daiichi-Sankyo, Janssen Pharma, Astra-Zeneca, Takeda Industrial Pharma, Astellas Pharma, Asahi-kasei Pharma and GlaxoSmithKline and has received research grant support from Mitsubishi-Tanabe Pharma, Bristol-Myers Squibb, Takeda Industrial Pharma, MSD, Astellas Pharma, Eisai Pharma, Chugai Pharma, Pfizer and Daiichi-Sankyo. The other authors declare no conflict of interest.

Patient consent Obtained.

Ethics approval Ethics approval was obtained from the committee in University of Occupational and Environmental Health, Japan.

Provenance and peer review Not commissioned; externally peer reviewed.

Received 9 March 2012
Accepted 3 May 2012

Published Online First 11 July 2012

Ann Rheum Dis 2012;**71**:2058–2059.
doi:10.1136/annrheumdis-2012-201657

REFERENCES

1. **Hamano H,** Kawa S, Horiuchi A, *et al*. High serum IgG4 concentrations in patients with sclerosing pancreatitis. *N Engl J Med* 2001;**344**:732–8.
2. **Masaki Y,** Dong L, Kurose N, *et al*. Proposal for a new clinical entity, IgG4-positive multiorgan lymphoproliferative syndrome: analysis of 64 cases of IgG4-related disorders. *Ann Rheum Dis* 2009;**68**:1310–15.
3. **Tanaka A,** Moriyama M, Nakashima H, *et al*. Th2 and regulatory immune reactions contribute to IgG4 production and the initiation of Mikulicz disease. *Arthritis Rheum* 2012;**64**:254–63.
4. **Punnonen J,** Aversa G, Cocks BG, *et al*. Interleukin 13 induces interleukin 4-independent IgG4 and IgE synthesis and CD23 expression by human B cells. *Proc Natl Acad Sci USA* 1993;**90**:3730–4.
5. **Umehara H,** Okazaki K, Masaki Y, *et al*. Comprehensive diagnostic criteria for IgG4-related disease (IgG4-RD), 2011. *Mod Rheumatol* 2012;**22**:21–30.
6. **Iwata S,** Yamaoka K, Niiro H, *et al*. Amplification of Toll-like receptor-mediated signaling through spleen tyrosine kinase in human B-cell activation. *J Allergy Clin Immunol* 2012;**129**: 1594–601.
7. **Khosroshahi A,** Bloch DB, Deshpande V, *et al*. Rituximab therapy leads to rapid decline of serum IgG4 levels and prompt clinical improvement in IgG4-related systemic disease. *Arthritis Rheum* 2010;**62**:1755–62.
8. **Deng GM,** Liu L, Bahjat FR, *et al*. Suppression of skin and kidney disease by inhibition of spleen tyrosine kinase in lupus-prone mice. *Arthritis Rheum* 2010;**62**:2086–92.
9. **Weinblatt ME,** Kavanaugh A, Genovese MC, *et al*. An oral spleen tyrosine kinase (Syk) inhibitor for rheumatoid arthritis. *N Engl J Med* 2010;**363**:1303–12.
10. **Podolanczuk A,** Lazarus AH, Crow AR, *et al*. Of mice and men: an open-label pilot study for treatment of immune thrombocytopenic purpura by an inhibitor of Syk. *Blood* 2009;**113**:3154–60.

A child with severe relapsing Kawasaki disease rescued by IL-1 receptor blockade and extracorporeal membrane oxygenation

Kawasaki disease (KD) is an acute inflammatory vasculitis that predominantly occurs in children under 5 years of age.[1] It is associated with the development of coronary artery aneurysms (CAA) in 15–25% of untreated cases.[2] Standard treatment consists of high-dose intravenous immunoglobulins (IVIG) along with aspirin.[3] About 15% of patients do not respond to a single dose of IVIG and need retreatment.[4] When ongoing signs of active disease are present, methylprednisolone pulses are often administered.[5] If there is a lack of response, alternative anti-inflammatory medication such as infliximab or plasmapheresis have been suggested in individual case series.[6 7] We report, for the first time, the beneficial use of an interleukin-1 receptor antagonist (IL-1RA) in relapsing KD.

CASE REPORT

A 2-year-old boy was presented with persistent fever, coughing and swollen cervical lymph nodes. The boy's condition had not improved with empirical antibiotic treatment. He developed a rash, conjunctivitis and swollen extremities. Upon admission the child was lethargic with increased C reactive protein (340 mg/l) (figure 1). KD was diagnosed, followed by IVIG administration (2 g/kg). Tachycardia and hypotension developed the next day. Echocardiography showed diminished shortening fraction of 20% without CAA. Two days later

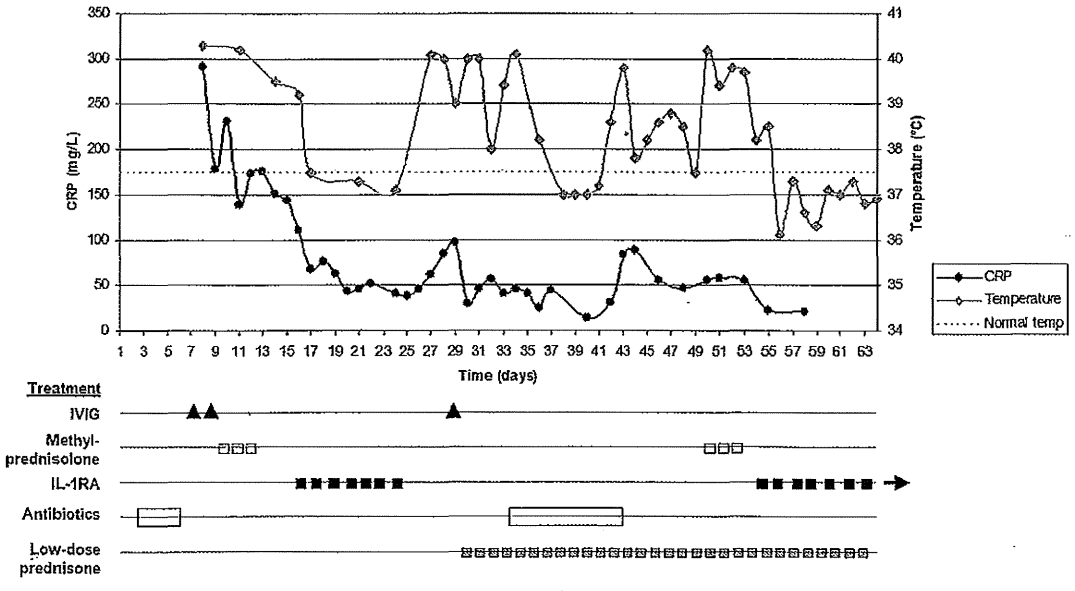

Figure 1 Time course of C reactive protein (CRP), temperature and treatment in a patient with severe treatment-resistant Kawasaki disease. Interleukin-1 receptor antagonist (IL-1RA) was administered in two episodes resulting in a prompt response. IVIG, intravenous immunoglobulin.